Division of Solid Mechanics

ISRN LUTFD2/TFHF–11/5161–SE (1-94)

SIMULATION AND TESTING OF GPHE CHANNEL PLATES DURING ASSEMBLING

Master's Dissertation by

Henrik Forsbäck and Joel Johansson

Supervisors
Ph. D. Håkan Hallberg, Div. of Solid Mechanics, Lund
M. Sc. Joakim Krantz, Alfa Laval Lund AB
M. Sc. Anders Lüning, Alfa Laval Lund AB

Examiner
Ph. D. Mathias Wallin, Div. of Solid Mechanics, Lund

Printed by Media-Tryck, Lund, Sweden.

For information, address:
Division of Solid Mechanics, Lund University, Box 118, SE-221 00 Lund, Sweden.
Homepage: http://www.solid.lth.se

Work distribution

In this master thesis all of the work have been made by Joel Johansson and Henrik Forsbäck.

Acknowledgements

This Master's Thesis was carried out at Alfa Laval Lund AB from September 2010 to March 2011 with supervision from the Division of Solid Mechanics, Lund University, Sweden.

The initiators of this project were M.Sc. Joakim Krantz, M.Sc. Johan Gidner and M.Sc. Anders Lüning at Alfa Laval. We would like to thank you all for the opportunity of making this project on site at Alfa Laval Lund AB. We are very grateful for the supervision, discussions and valuable support throughout the project.

We would like to thank our supervisor at the Division of Solid Mechanics, Ph.D Håkan Hallberg, for his feedback and guidance during the project. We would also send our gratitude to Zivorad Zivkovic for giving us the chance to perform tests in the Division of Solid Mechanics lab at Lund Institute of Technology.

Many thanks to the colleagues at Alfa Laval, Fredrik Andreasson and his team at the Concept department for producing and helping us with the pressing tool for our practical tests and to Ola Ekström and his team at the MACC department for their support and help with the tensile test machine.

Lund, March 2011
Henrik Forsbäck and Joel Johansson

Abstract

The objective of this thesis is based on a continuous desire from Alfa Laval to optimize the development of their product portfolio. To further optimized their devices, there is interest for a more profound understanding of how the plates in the heat exchanger occurs under load. When assembling a plate heat exchanger the ambition is to obtain metallic contact points in the plate package, consisting of channel plates that are compressed. The metallic contact that occur will vary depending on how plates locally deform, which in turn depends on the plate geometry and rigidity. The main variance of the plates consists of an allowable tolerance for the thickness and pressure depth. To examine this behavior both simulations and experimental tests were conducted.

The requirement for the simulations was that they would be performed in ANSYS Workbench, software for finite element analysis. In the simulations the objective was to include features such as plastic strains, residual stresses and impressing of plate material. These were divided into three models with increasingly more complex layout. Imitation of the processes that occur at the assembly stage, i.e. first pressing of the plate followed by the compression of the same, was completed in the simulations using multi-step analysis.

It turned out to be difficult obtaining satisfactory results for this type of simulations in ANSYS Workbench. The models implemented expose above all a stiffer performance than reality shows. The conclusion has been drawn for this, that much of the effects of the boundary conditions are not equivalent with what happens in reality.

The experimental tests were conducted in a tensile testing machine, used for compression instead of tension. In order to apply the test in the machine a fixture was required. This fixture allowed us to carry out tests both with and without a boundary box, a restriction that prevents expansion in the transverse direction of the plate. The tests were divided into single and multi-plate test. This refers to the number of plates used in the fixture during testing. There were also tests performed to show the effect of this restricting boundary box. The conclusion of the experimental test is that a limitation of the boundary has a relatively small effect on the result when several plates are pressed together. This because of that the deformation occurs mainly in local deformations. Finally, the stiffness responses for the various plate thicknesses are shown. That result is then used to present which effect a change in tolerance level would give upon the needed assembly force.

Sammanfattning

Uppkomsten av detta examensarbete grundar sig på en ständig strävan hos Alfa Laval att optimera sin utveckling av sitt produktsortiment. För att vidare optimera sina apparater finns det intresse för en djupare förståelse för hur plattorna i dessa värmeväxlare uppträder under belastning. Vid ihopspänningen av en plattvärmeväxlare strävas det efter att få metalliska kontaktpunkter i det plattpaket, bestående av kanalplattor, som finns inspänt. Den metalliska kontakt som uppstår kommer att variera med avseende på hur plattorna lokalt deformeras, vilket beror på plattornas geometri och styvhet. Måttvariansen för plattorna består i ett tillåtet toleransvärde för tjockleken respektive pressdjupet. För att undersöka effekten av att ändra dessa toleransvärden genomfördes både simuleringar och experimentella test.

Kravet för simuleringarna som genomfördes var att de skulle utföras i ANSYS Workbench, en programvara för finita element analyser. Vid simuleringarna var målet att få med aspekter som plastiska töjningar, restspänningar och prägling av plattmaterialet. Dessa delades upp i tre modeller med en successivt komplexare uppställning. Imiteringen av de processer som sker vid monteringsfasen, det vill säga, först en pressning av plattan följt av komprimeringen av den samma, gjordes i simuleringarna med hjälp av flerstegsanalyser. Det visade sig vara svårt att få tillfredställande resultat för den här typen av simuleringar i ANSYS Workbench. De modeller som genomförts visar framförallt på ett styvare resultat än vad verkligheten visar på. Slutledningen som har dragits för detta är att effekten från randvillkoren inte är ekvivalenta med vad som händer i verkligheten.

De experimentella testen genomfördes i en dragprovsmaskin som utnyttjades för att trycka ihop testobjekten. För att kunna applicera testen på maskinen krävdes att en fixtur tillverkades för att hålla platterna på plats. Denna fixtur tillät oss att genomföra test både med och utan en låst rand, där en låsning innebär att utvidgningen i tvärled av plattan förhindrades.

Testen delades in i en- och flerplattstest. Detta syftar till hur många plattor som samtidigt var i fixturen vid testningen. Det gjordes också test för att försöka påvisa den effekt som en låst rand innebär. Sammantagningen av de experimentella testen är att en inlåsning har en relativt liten effekt på resultatet när flera plattor trycks ihop eftersom deformationen sker framförallt i lokala deformationspunkter mellan plattorna. Slutligen visas de styvhetsresponser som de varierande plattjocklekarna gav upphov till samt vad en förändring i toleransnivå ger för effekt på ihopspänningskraften.

Contents

Chapter 1

Introduction

The following chapter is an introduction to the project objective. The first section gives a presentation of Alfa Laval, their major technologies and why this project was established. The following sections describe the project formulation, its objective and the limitations set for this dissertation.

Figure 1.1: Plate heat exchanger

1.1 Alfa Laval

The origin of Alfa Laval dates back to 1883, when Gustaf de Laval founded the company to exploit his pioneering invention of the centrifugal separator. Today, Alfa Laval's equipment, systems and services are hard at work in more than a hundred countries. To create a clear focus on different types of customers, Alfa Laval's business is divided into ten segments, this to give insight into their special needs and the strength to develop the best possible solutions to fulfill them. Alfa Laval has 28 production sites and 55 service centres spread all over the world with approximately 11500 employees worldwide.

The Alfa Laval brand stands for technical expertise, reliable products, efficient service and the finest process engineering skills. Its reputation is based on their unique knowledge and experience in the three key technologies of separation, heat transfer and fluid handling, which play major roles in most sectors of industry.

- *Separation*
  Alfa Laval has led the development of separation technology since the company was founded in 1883. Today Alfa Laval is the world's largest supplier of separation solutions.
- *Heat Transfer*
  Alfa Laval is the world leader in plate and spiral heat exchangers. The company also offers the market's most extensive range of refrigeration equipment.
- *Fluid handling*
  Alfa Laval produces flow equipment for industries requiring high standards of hygiene and reliable, continuous flows.

1.2 Background

Since the project was carried out at Alfa Laval in Lund, which is responsible for the product range of brazed and gasketed plate heat exchangers, the plate heat exchanger was the apparatus type that was relevant for the project.

A gasketed plate heat exchanger, GPHE, consists of a number of corrugated plates, known as channel plates, with openings for two or more heat exchanging fluids. To avoid mixing the fluids, rubber gaskets separate them into different channels. The plate package ends with frame plates which are held together with tightening bolts to prevent leaking.

During the last decades the introduction of finite element analyses have provided a more precise tool for the development of plate heat exchangers. The simulations results in an even more optimized frame design, which despite its modest dimensions is capable higher stresses than before.

This never ending design optimization ensures that Alfa Laval can continue to deliver cost-effective and competitive products to market. To carry on these optimizations Alfa Laval requires further knowledge about the channel plate package and how it performs during assembling.

1.3 Objective

The major focus of this report is to study how support points are established between the channel plates during assembling. A support point is a mechanical contact between two channel plates that is necessary for the rigidity of the plate heat exchanger. This topic is then transformed into two parallel sections.

The first part investigates how to implement a computer-aided simulation that express the sequence of events during assembly of a plate heat exchanger. These simulations should be performed with the use of finite element analysis. The finite element software for solving these analyses is ANSYS Workbench 12.1.

The second part is to explore how the channel plates physically behave through experimental tests. This testing part includes all steps from decisions about the testing tool design, test specification to performance of the experimental testing. The tests have been performed at the department Materials and Chemistry Centre, Alfa Laval Lund on a tensile test machine. Some tests were also conducted at the Division of Solid Mechanics lab at Lund Institute of Technology.

The channel plates used as testing material are made of stainless steel grade 316, cold rolled sheets. This material represents a typical example for this optimization studies. The stainless steel is commonly used and more or less isotropic which makes it good for this initial study. Even though the rolling direction of the material affect the isotropic properties, Alfa Laval believes that this influence is negligible.

The plate apparatus is a product in a field of products having the same type of corrugated plate pattern. A field where Alfa Laval wants increased knowledge.

1.4 Delimitations

The influence of the gaskets is excluded from the topic of this project. Due to previous studies done at Alfa Laval on the gaskets, the gasket response is considered as fully known and will be excluded of this thesis.

The type of plate patterns that were examined in the project consisted only of chevron patterns with the characteristics of low pressing depth. No studies were performed at the distribution surface of the plates.

A request from Alfa Laval was to evaluate the use of a specific software for this type of application, and hence that the project is limited to use ANSYS Workbench 12.1.

Chapter 2

Gasketed Plate Heat Exchanger

For the reader to understand the concepts and assumptions that are introduced continuously in this report, understanding of how a plate heat exchanger is designed and the various components which it is built upon is required.

This chapter begins by explaining the working principle of a general plate heat exchanger and which parts it consists of. The section is concluded by focusing on how the channel plates interact from a mechanical point of view.

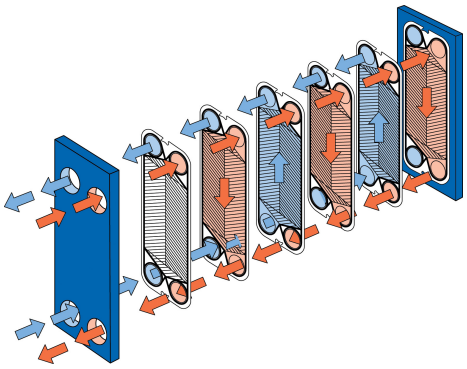

Figure 2.1: Flow path of the fluid.

2.1 General Principle

The concept behind a plate heat exchanger (PHE) is the use of separated chambers that allows heat transfer between two fluids without mixing them. One could for example pasteurize milk with the use of hot water without diluting the milk itself.

A gasketed plate heat exchanger uses, as briefly described in the background text, multiple gasket separated corrugated plates to establish these separated containing chambers, or flow channels. The gasket seals the interplate channel and forces the medium to flow parallel between every other plate, see figure 2.1. The plates are made of pressed sheet metal because of this material's high thermal conductivity and ductility. Together with a low thickness of the metal plates one ensures a rapid heat transfer.

To ensure that the plate package does not leak it is compressed until the point were the gaskets seal it, and then mounted in a rigid frame. This design has a major advantage in that the fluid is exposed to a very large surface. This facilitates the heat transfer and increases the rate of temperature change.

2.2 Plate pattern

During the past century more than 60 different corrugation patterns have been developed worldwide [6]. According to Bengt Sundén [7] the chevron, or herringbone, pattern is the most prevalent one due to its performance. This pattern has been shown to provide good thermal and hydraulic characteristics, while still providing a rigid mechanical design. Mechanical properties of different corrugation patterns are discussed in more detail in the next section "2.2 Package Rigidity".

The corrugated pattern of the plate forms grooves in an angle to the flow, and force the fluid into turbulence. This design, together with a thin plate chamber, ensures that the majority of the fluid volume is in contact with the plate surface which in turn aids the heat exchange.

The inclination angle of the grooves with respect to the main flow direction has been shown in several tests to be an important design parameter, with respect to fluid friction and heat transfer [2]. Therefore, to be able to cope with the pressure levels and flow rates demanded by the market, the plate in question is manufactured in several versions and varies in both thickness and inclination angle. The plates tested in this report are selected by Alfa Laval and have the thicknesses 0.4, 0.5 and 0.6 millimeters, and two different angles, θ_{high} and θ_{low}. In figure 2.2 the plate thickness and inclination angle are defined of two plates stacked upon each other. Moreover, the press depth of the chevron pattern, which is related to later on, is also defined. One should notate that the press depth do not include the plate thickness.

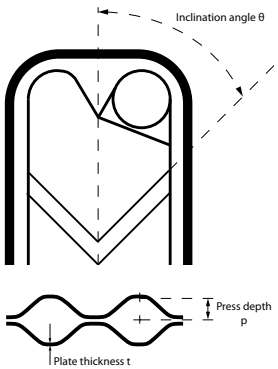

Figure 2.2: Plate thickness, press depth of the pattern and the inclination angle

The plate has a design of two main zones, the heat surface where the heat exchange occurs (A), and the end areas of the plate (B) which ensure a proper distribution of the fluid to the heat surface, see figure 2.2. The plates are then stacked on top of each other, each rotated 180 degrees from its neighbors, forming several flow paths between the two plates. One could also in figure 2.2 notice the typical gasket design, which ensures that the two fluids enter every second flow channel.

Due to that the heat surface represents a major proportion of the plate's total area it is reasonable to assume that this also represents the largest part of the plate's properties. This, combined with the consistency of the pattern, provides a good basis for further analysis of the plate characteristics when load is applied. For these reasons, this work focuses mainly on the heating surface.

Package Rigidity

When the heat exchanger is assembled the plates are subjected to design pressure loads of up to 30 Bar. One of the problems designers have to address is to model a plate that is capable to handle loads without showing any local deformation and still contain suitable thermal properties. Due to the nature of the PHE's design the largest strains occur when the plate is subjected to differential loads. This occurs at assembly when the GPHE's are subjected to

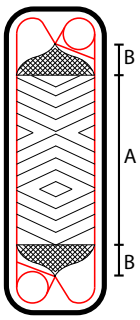

Figure 2.3: The heat surface (A), the distribution areas (B) of the plate pattern and the gasket in red.

a test pressure, which is chosen higher than the normal operating pressure.

To handle this problem the pattern is designed so that the grooves form several contact points with the next plate and establish rigidity and mechanical support through the plate package. As the thickness and pressing depth is fixed at a plate, the inclination angle of the chevron pattern determines the density of these contact points and thus the strength of the plate. This means that the designer needs to model enough contact points to bear the load, but without increasing the flow resistance beyond the specified level determined from thermal calculations.

To make sure that the plate package do not leak, the package is contracted to a specified nominal length during assembly, the so called *A-length*, see figure 2.4. At this nominal length the gaskets are fully compressed and the channel plates have formed mechanical contacts trough the whole package. It should be a reasonable assumption that almost the entire load that is generated due to fluid pressure is admitted to the plates and the contact between them, rather than in the gaskets.

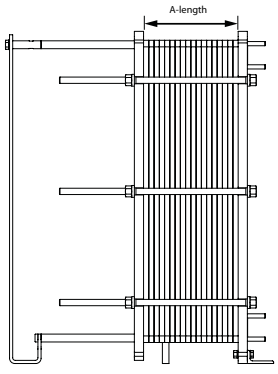

Figure 2.4: The PHE is contracted to A-length during assembly, to ensure correct product properties.

Chapter 3

Theory

The following chapter describes the theoretic basis of the computer simulations used in this thesis. The reader is assumed to have a basic understanding of solid mechanics.

3.1 Material Description

As mentioned before the material of the plates is stainless steel of grade 316. The grade 316 follows a standardization based on the crystal structure and the composition of added chemical elements that the actual material has.

The characteristics of grade 316 are excellent for forming and welding which makes it perfect for heat exchanger applications. It has a good resistance against corrosion which can be necessary in many aggressive environments e.g. applications including dairy, food and beverage, and other sanitary processes.

For this thesis the material properties were given in terms of tensile test data. This data describe the uniaxial material relation in a true stress-strain curve. This data shown in figure 3.1 is representative for this kind of steels and contains typical behaviors for elastic and plastic deformations. The characteristic yield stress for these steel types is typically 200-300 MPa, and this is fulfilled by the given data from Alfa Laval.

The material response of steels like this can be considered as independent of direction, which is known as isotropic behavior. This isotropy will be further explained in section 3.3.1.

3.2 Elasticity

The simplest form of a constitutive model is when the behavior of the material is assumed to be linearly elastic. This relation is in one dimension expressed by Hooke's law.

$$\sigma = \mathbf{E} \cdot \varepsilon^{\mathbf{e}} \tag{3.1}$$

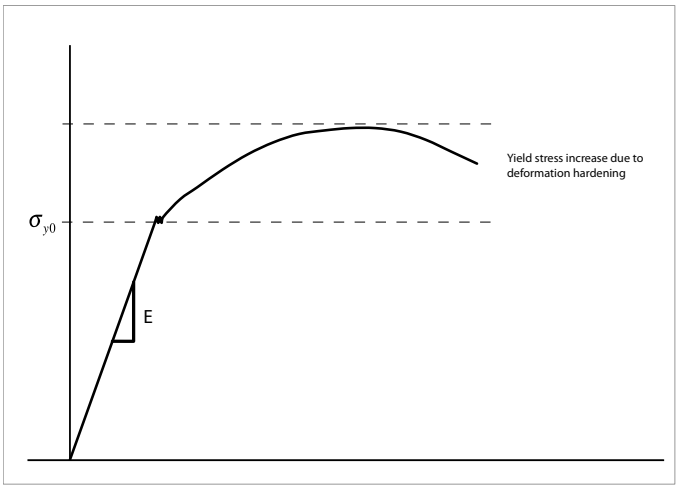

Figure 3.1: General steel tensile test

where E is a material constant known as Young's modulus. This parameter sets the relation between the stress and the strains and corresponds to the slope of the curve, see figure 3.1. The superscript e indicates that the strain in this relation should be only elastic. The corresponding expression to the general three dimensional case is then stated as

$$\sigma = \mathbf{D}\varepsilon \tag{3.2}$$

where $\mathbf{D}$ is the stiffness tensor corresponding to the one dimensional E, and σ is *Cauchy stress tensor*. This expression is known as *Hooke's generalized law*.

3.3 Elasto-plasticity

When introducing plastic deformations these are beyond the linear elastic region. A plasticity model is then needed to cover situations where the material is loaded above the *yield stress*, σ_y. I.e. where strains still exists in the body after unloading.

To describe the behavior when $\sigma > \sigma_y$ a so called yield function has to be introduced. This function may be linear or non-linear, dependent on the load history and can vary according to what material one is studying.

A typical characteristic for steel materials is deformation hardening. In other words increased deformation makes the steel harder. A general description of how this appear in the one dimensional case is shown in figure 3.1. Assuming isotropic hardening, can be applied to the yield function as a hardening parameter.

The yield function or in this case yield surface can be expressed as

$$f(\sigma, K) = 0 \tag{3.3}$$

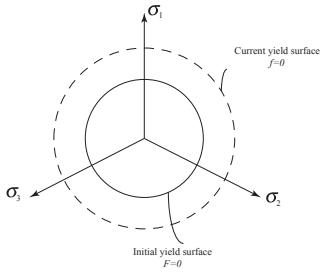

Figure 3.2: Von Mises hardening

where $K = 0$ gives the initial yield surface. This hardening parameter or parameters can be varied to get the property of the material that one are searching for.

3.3.1 Isotropic hardening

Typical hardening for ductile materials such as metals and steel (that is not exposed to cyclic loading) is an isotropic hardening model. The most common criterion used for this yield function is the *von Mises criterion* where the initial yield surface is given by

$$\sigma_{eff} = \sqrt{3J_2} \tag{3.4}$$

$$F(\sigma_{ij}, K) = \sigma_{eff} - \sigma_{y0} = 0 \tag{3.5}$$

where J_2 is the second invariant of the deviator stress tensor and

$$J_2 = \frac{1}{2} s_{ij} s_{ij} \tag{3.6}$$

where

$$s_{ij} = \sigma_{ij} - \frac{1}{3}\sigma_{kk}\delta_{ij} \tag{3.7}$$

is the deviatoric part of the stress tensor.

The Kronecker delta is denoted by δ_{ij}. In this case the hardening parameter K is a function of κ, describing the development of the plastic strains and memorizing thereby the plastic loading history. At elastic loadings $K(\kappa)$ is equal to zero. The yield criterion can now be formulated as

$$\mathrm{f}(\sigma,\kappa) = \sigma_{eff} - \sigma_y(\kappa) = 0; \quad \sigma_y(\kappa) = \sigma_{y0} + K(\kappa) \tag{3.8}$$

This constitutive model will represent an isotropic hardening as seen in figure 3.2. If $\sigma_{eff} < \sigma_y$ the material response is elastic and the stresses will develop according to the elastic stress-strain relation. When loading exceeds the elastic range plastic deformations occur. The yield surface must then expand to keep the function equal to zero.

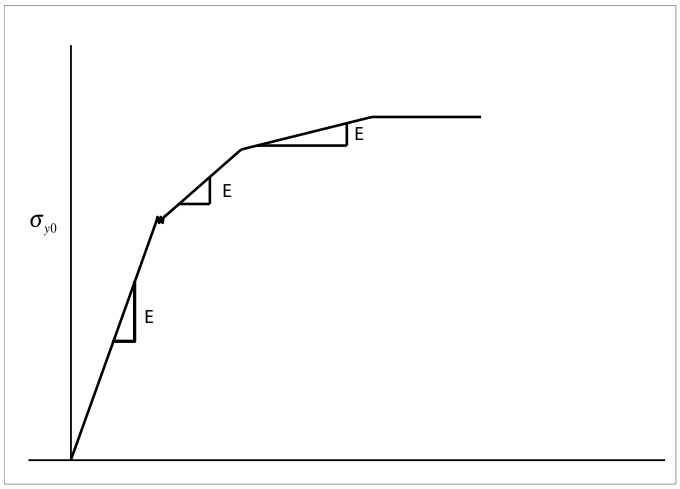

Figure 3.3: Multi linear isotropic hardening

3.3.2 Multi linear isotropic hardening

There is a few alternatives to simulate the nonlinear isotropic hardening described in "3.3.1 Isotropic hardening" when implementing the theoretical description of isotropic hardening into ANSYS Workbench.

- Bilinear Isotropic Hardening
- **Multi linear Isotropic Hardening**
- Nonlinear Isotropic Hardening

The one chosen for this master thesis is the Multi linear isotropic hardening. This was used because of the simple implementation using the given material data, see figure 3.3. The material data contains a large number of data points. Between these points the Multi linear model will interpolate linearly the gaps to get a continuous function. Due to the high resolution of points the linearization is assumed not to affect the curvature in any critical way which makes it a good approximation for the problem.

When stresses above the yield strength occur in the simulations the actual plastic strain state will be calculated according to this curvature.

3.4 The finite element method

This chapter introduces the reader to the finite element method. This is an efficient numerical solution method for physical engineering problems. The obtained numerical solution is an approximation to the analytical problem but to many problems it is very hard or even impossible to calculate the analytical solution and then the approximation may satisfy ones needs.

The method applies finite elements to the area, volume or body that the problem involves. This collection of small divisions of the total body is called the finite element mesh. The differential equations will the be solved for each and every element to obtain the solution. The interested reader is referred to Ottosen and Ristinmaa [4].

3.4.1 Strong formulation

To establish the finite element formulation the equations of motion, i.e. the principle of virtual work for an arbitrary body, is used. This states that all forces working on a body will be equal to the mass of the body times the acceleration. The formulation is done with assumptions of small displacements.

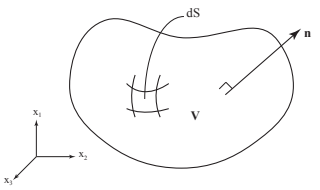

Figure 3.4: Volume V with surface boundary S and outer normal unit vector **n**

$$\int_s t_i dS + \int_v b_i dV = \int_v \rho \ddot{u}_i dV \tag{3.9}$$

Where t_i is the traction vector describing the load applied to the body along the surface S , b_i is the body forces defined as force per volume, ρ is the density of the body, dot accent indicates the time derivate and $\ddot{u}_i$ is then the acceleration. The traction vector t_i can be reformulated with *Cauchy's formula* where

$$t_i = \sigma_{ij} n_j \tag{3.10}$$

including n_j which is the plane normal vector. To reformulate this the *Gauss divergence theorem* is introduced. This states the following relation for an arbitrary vector q_i.

$$\int_V q_{i,i} dV = \int_S q_i n_i dS \tag{3.11}$$

where

$$q_{i,i} = \frac{\partial q_i}{\partial x_i} \tag{3.12}$$

The reformulated expression is then obtained as

$$\int_V (\sigma_{ij,j} + b_i - \rho\ddot{u}_i)dV = 0 \tag{3.13}$$

Since this equations is defined for arbitrary bodies, this balance equations can be reduced to the so called *strong formulation*.

$$\sigma_{ij,j} + b_i = \rho\ddot{u}_i \tag{3.14}$$

3.4.2 Weak formulation

The principle of virtual work or equally the weak formulation can be applied to any balance equation. To establish this, the equations of motion are multiplied with an arbitrary vector, the *weight vector* v_i and then integrated over the body

$$\int_V v_i\sigma_{ij,j}dV + \int_V v_i b_i dV = \int_V v_i\rho\ddot{u}_i dV \tag{3.15}$$

By using the derivative rules of a product on the first term in (3.15) this can be expressed as

$$\int_V v_i\sigma_{ij,j}dV = \int_V [(\sigma_{ij}v_i)_{,j} - \sigma_{ij}v_{i,j}]dV \tag{3.16}$$

and as before the first of the new terms may be reformulated with the Gauss divergence theorem as

$$\int_V (\sigma_{ij}v_i)_{,j}dV = \int_S \sigma_{ij}v_i n_i dS = \int_S v_i t_i dS \tag{3.17}$$

By applying this substitutions to equation (3.15), the weak formulation is obtained as

$$\int_S v_i t_i dS - \int_V v_{i,j}\sigma_{ij}dV + \int_V v_i b_i dV = \int_V v_i\rho\ddot{u}_i dV \tag{3.18}$$

The kinematic relation for the strain tensor known as *Green strain* is stated as

$$\varepsilon_{ij} = \frac{1}{2}(u_{i,j} + u_{j,i} + (u_{k,i}u_{k,j})) \tag{3.19}$$

The last quadratic term is excluded when handling small strains since it will be negligible. From equation (3.19) it is convenient to introduce the tensor ε^v_{ij} as an relation to the arbitrary vector v_i. This has no physical significance and is just a quantity defined.

$$\varepsilon^v_{ij} = \frac{1}{2}(v_{i,j} + v_{j,i}) \tag{3.20}$$

With this the weak form of equations of motion is

$$\int_V v_i\rho\ddot{u}_i dV + \int_V \varepsilon^v_{ij}\sigma_{ij}dV = \int_S v_i t_i dS + \int_V v_i b_i dV \tag{3.21}$$

3.4.3 Deriving FE-formulation

As the last expression of the weak form is written in index notation this section starts with a translation to matrix notation and an identification of the involved components.

The weak formulation from (3.21) is then

$$\int_V \rho \mathbf{v}^T \ddot{\mathbf{u}} dV + \int_V (\boldsymbol{\varepsilon}^{\mathbf{v}})^T \mathbf{s} dV = \int_S \mathbf{v}^T \mathbf{t} dS + \int_V \mathbf{v}^T \mathbf{b} dV \tag{3.22}$$

where

$$\boldsymbol{\sigma} = \begin{bmatrix} \sigma_{11} \\ \sigma_{22} \\ \sigma_{33} \\ \sigma_{12} \\ \sigma_{13} \\ \sigma_{23} \end{bmatrix} \quad \boldsymbol{\varepsilon}^{\mathbf{v}} = \begin{bmatrix} \varepsilon^v_{11} \\ \varepsilon^v_{22} \\ \varepsilon^v_{33} \\ 2\varepsilon^v_{12} \\ 2\varepsilon^v_{13} \\ 2\varepsilon^v_{23} \end{bmatrix} \quad \ddot{\mathbf{u}} = \begin{bmatrix} \ddot{u}_1 \\ \ddot{u}_2 \\ \ddot{u}_3 \end{bmatrix}$$

$$\mathbf{v} = \begin{bmatrix} v_1 \\ v_2 \\ v_3 \end{bmatrix} \quad \mathbf{t} = \begin{bmatrix} t_1 \\ t_2 \\ t_3 \end{bmatrix} \quad \mathbf{b} = \begin{bmatrix} b_1 \\ b_2 \\ b_3 \end{bmatrix} \tag{3.23}$$

The finite element method is based on an approximated relation so-called *global shape functions*. These express that the displacement vector $\mathbf{u}$ throughout the body depending on both time and position can be related to the global shape functions $\mathbf{N}$ depending on time and the *nodal displacements* of the body, denoted $\mathbf{a}$ depending on position.

$$\mathbf{u}(x_i, t) = \mathbf{N}(x_i)\mathbf{a}(t) \tag{3.24}$$

The interpolation between the displacement vector and the nodal displacements is defined through the choice of approximation method.

With equation (3.19) the corresponding strains are then specified as

$$\boldsymbol{\varepsilon}(x_i, t) = \mathbf{B}(x_i)\mathbf{a}(t) \tag{3.25}$$

The $\mathbf{B}(x_i)$ matrix is derived from the global shape functions and is in the same way depending on position. The remaining component to declare is the weight vector $\mathbf{v}$. A suitable way of defining this is in accordance with the *Galerkin method*. The weight vector is approximated in the same manner as the global displacement vector, which leads to

$$\mathbf{v}(x_i, t) = \mathbf{N}(x_i)\mathbf{c}(t) \tag{3.26}$$

The introduced vector $\mathbf{c}$ will also be arbitrary since $\mathbf{v}$ is arbitrary and $\mathbf{N}$ is defined. If one make use of the relation between $\boldsymbol{\varepsilon}$ and $\mathbf{u}$, then $\boldsymbol{\varepsilon}^{\mathbf{v}}$ can be expressed as

$$\boldsymbol{\varepsilon}^{\mathbf{v}} = \mathbf{B}\mathbf{c} \tag{3.27}$$

If one inserts the defined quantities in the weak formulation from equation (3.22) this gives

$$\mathbf{c}^T \left[(\int_V \rho \mathbf{N}^T \mathbf{N} dV)\ddot{\mathbf{a}} + \int_V \mathbf{B}^T \boldsymbol{\sigma} dV - \int_S \mathbf{N}^T \mathbf{t} dS - \int_V \mathbf{N}^T \mathbf{b} dV \right] = 0 \quad (3.28)$$

Since $\mathbf{c}$ is an arbitrary vector the expression inside the brackets must also be equal to zero. To complete the finite element formulation a constitutive relation is required. For this example of derivation the elastic relation known from (3.2) is used and reformulated as

$$\boldsymbol{\sigma} = \mathbf{D}\boldsymbol{\varepsilon} = \mathbf{DBa} \quad (3.29)$$

To express the final formulation in a compact manner three definitions are made.

The mass matrix:	$\mathbf{M} = \int_\mathbf{V} \rho \mathbf{N^T N dV}$
The stiffness matrix:	$\mathbf{K} = \int_\mathbf{V} \mathbf{B^T D B dV}$
The external force vector:	$\mathbf{f} = \int_\mathbf{S} \mathbf{N^T t dS} + \int_\mathbf{V} \mathbf{N^T b dV}$

The finite element formulation is then obtained as

$$\mathbf{M}\ddot{\mathbf{a}} + \mathbf{Ka} = \mathbf{f} \quad (3.30)$$

If the simulation is static, there is no time-dependent and the first term $\mathbf{M}\ddot{\mathbf{a}}$ is therefore disregarded.

To this *boundary conditions* are added. They contain prescribed conditions to the body. Like a defined displacement at the boundary surface $\mathbf{S_u}$ or a prescribed traction vector along the boundary surface $\mathbf{S_t}$ affecting the body.

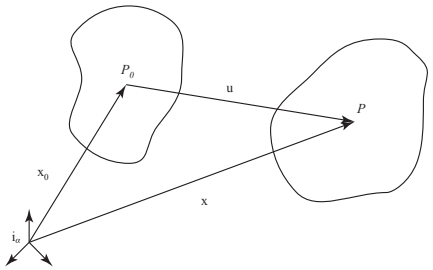

Figure 3.5: Displacement $\mathbf{u}$ from initial configuration $\mathbf{x_0}$ to current configuration $\mathbf{x}$

3.5 Large deformations

When deformations are small the linear small strain tensor and the corresponding Cauchy stress are suitable to use as approximations for the formulation. For the small strain theory the deformation of the body is defined from the initial configuration added by the displacement of the arbitrary point by vector u ending up in the current configuration, see figure 3.5. When introducing large deformations or so-called finite deformations one make instead use of the deformation gradient tensor $\mathbf{F}$. This deformation gradient is defined by the relation

$$d\mathbf{x} = \mathbf{F}\mathbf{dx_0} \tag{3.31}$$

where $\mathbf{x}$ is in the current configuration and $\mathbf{x_0}$ is in the initial configuration. The index 0 is to point out that the expression is referring to the initial configuration. Recalling the Green strain from (3.19) one can define the *Green finite strain tensor* in a three dimensional manner as

$$\mathbf{E} = \frac{\mathbf{1}}{\mathbf{2}}(\mathbf{D} + \mathbf{D^T}) + \frac{\mathbf{1}}{\mathbf{2}}\mathbf{D^T}\mathbf{D} = \frac{\mathbf{1}}{\mathbf{2}}(\mathbf{F^T}\mathbf{F} - \mathbf{I}) \tag{3.32}$$

For convenience $\mathbf{E}$ is written as a vector

$$\mathbf{E} = \begin{bmatrix} E_{11} \\ E_{22} \\ E_{33} \\ 2E_{12} \\ 2E_{13} \\ 2E_{23} \end{bmatrix} \tag{3.33}$$

To define the corresponding stress tensor for finite deformations the approach is very similar. In relation to the Cauchy's formula which is defined in the current configuration a definition of a relation in the initial configuration is done.

$$\mathbf{t}_0 = \mathbf{P}\mathbf{n}_0 \tag{3.34}$$

The introduced matrix $\mathbf{P}$ is known as the *first Piola-Kirchoff stress tensor*. Further it can be shown that the relation between the Cauchy stress and the

first Piola-Kirchoff is

$$\mathbf{P}{=}J\sigma\mathbf{F}^{-T} \tag{3.35}$$

$$J = det(\mathbf{F}) \tag{3.36}$$

where J is the Jacobian to the deformation gradient $\mathbf{F}$. Since this tensor is not symmetric it is convenient to define the *second Piola-Kirchoff stress tensor*. This has the property of being energy conjugated to the Green finite strain tensor and is expressed as

$$\mathbf{S} = J\mathbf{F}^{-1}\sigma\mathbf{F}^{-T} \tag{3.37}$$

Similar to the Green finite strain tensor this is usually presented as

$$\mathbf{S} = \begin{bmatrix} S_{11} \\ S_{22} \\ S_{33} \\ S_{12} \\ S_{13} \\ S_{23} \end{bmatrix} \tag{3.38}$$

3.6 Element theory

This section describes the underlying theory of those element types which have been used by the ANSYS software during the simulations. This chapter focuses on mainly two element types, the solid elements and the contact element. The latter can be divided into two parts which concern the contact surface and the target surface. Finally, we also explain the different types of mathematical algorithms designed to describe the contact process.

During the preprocesses of the simulations that have been done during this master thesis the ANSYS software chose the suitable element types automatically.

Solid elements are three-dimensional finite elements that are used to model solid geometries. Each node has three degrees of freedom according to the three translation directions (x y z), corresponding to the simulation coordinate system. This element type can thereby model a full three-dimensional stress state.

To help the reader understand the element type descriptions presented later in this chapter, some keywords are explained shortly.

3.6.1 Shape functions

As described in section 3.4.3 the finite element calculations are based on the nodal displacement. To describe the displacement of the whole body, the shape function interpolate the nodal displacement over the element. The shape functions are often a polynomial function (as linear or quadratic) and the polynomial degree determines what the global displacement field will look like.

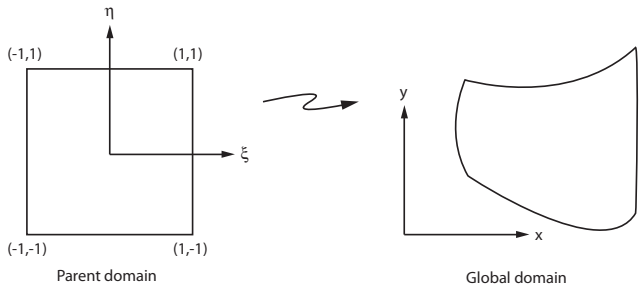

Figure 3.6: Isoparametric mapping

3.6.2 Isoparametric mapping

In order to allow the elements to deform freely and not stay limited to being parallel to the coordinate system, isoparametric mapping is introduced. A region, called *parent domain*, with a local $\xi\eta$-coordinate system, holds an undeformed isoparametric finite element. Later on this element is mapped to a *global domain* region which allows a deformed element in the global xy-coordinates, see figure 3.6.

While introducing the shape functions in the parent domain, one encounters problems when trying to evaluate the stiffness matrix $\mathbf{K}$. The $\mathbf{B}$-matrix (eq. 3.25) is obtained by differentiating the shape function $\mathbf{N}$ with respect to x and y, but due to the isoparametric formulation the shape functions are now expressed in terms of $\xi\eta$-coordinates. This gives rise integrals that are difficult to solve analytically. To get around this problem one could approximate the integrals with so-called *numerical integration techniques* [3].

3.6.3 Gauss integration points

The use of isoparametric elements forces one to use an approximate manner to solve difficult integrals. While there are several methods to achieve this, the most commonly used is the *Gauss integration scheme* [3]. To acquaint the reader with the concept, we present a brief summary of the methodology. Consider the problem

$$I = \int_{-1}^{1} f(\xi) d\xi \tag{3.39}$$

where $f(\xi)$ is a arbitrary function and I is the integral quantity that is difficult to solve analytically. Similar to a Riemann sum we can approximate this by selecting some points ξ_i in the interval $-1 \leq \xi \leq 1$, called *integration points* [5].

$$I = \sum_{i=1}^{n} f(\xi_i) H_i + \mathrm{R} \tag{3.40}$$

The term H_i refers to a *weight parameter* and R to the *remainder*, see figure 3.7. By choosing the integration points and the weight parameters correct one

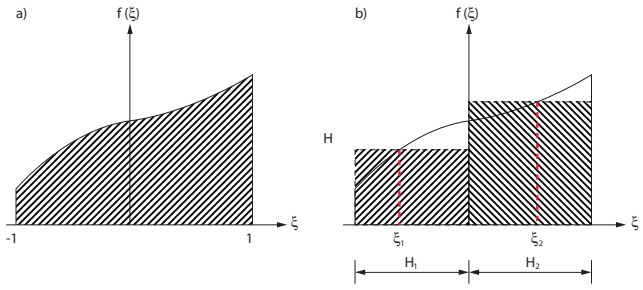

Figure 3.7: Gauss integration

could reduce the remainder to zero. One way of doing this is by using predefined *Gauss* points and corresponding weights. It can be shown that [3]

> For n integration points, Gauss integration provides an exact integration of a polynomial of the order $2n-1$.

In simplified terms we speak of *full integration* when the number of Gauss points is chosen to give an exact solution. Any integration of a lower order than this is referred to as a *reduced integration*.

Although ANSYS software has several element types to choose from, only two varieties of solid elements were used in the simulations. The software itself chose the appropriate elements to the performed simulations, the so-called SOLID186 and SOLID187.

SOLID186 - 3D 20-Node Structural Solid

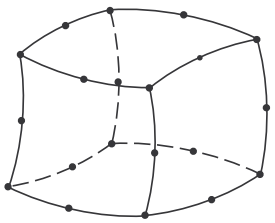

Figure 3.8: SOLID186 - 3D 20-Node Structural Solid

This element is a high order, three-dimensional, solid type which suits well for modeling the irregular meshes that are needed for the plate geometry. Solid186 has a quadratic displacement behavior due to the midside nodes and is able to model several conditions as for example: plasticity, large strains and large deflections. Pressure loads are defined as positive when acting into the element and are applied at the nodal points, marked as black circles in figure 3.8. For a full list of definitions and configuration choices, the reader is directed to Appendix A.1.

SOLID187 - 3D 10-Node Structural Solid

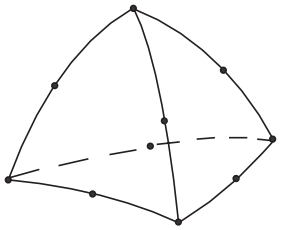

Figure 3.9: SOLID187 - 3D 10-Node Structural Solid

This variant is a tetrahedral element with much in common with the SOLID186 element. It can be used as an alternativ element when meshing irregular geometries. Pressure loads are defined as positive when acting into the element and are applied at the nodal points, marked as black circles in figure 3.9. For a full list of definitions and configuration choices, the reader is directed to Appendix A.2.

3.7 Contact formulation

When modeling geometries with more than one part, one will eventually have to face the problem with interactions between the bodies. For example this could be in terms of magnetic coupling, heat transfer between surfaces or rigid/elastic mechanical contact. There are several ways to formulate a body to body contact which this dissertation will not cover, but the fundamentals will be presented. First, the contact concept is explained, then two solving methods are discussed and then the used contact elements in ANSYS are presented. The derivation behind the following formulations can be read about further in the article by Kloosterman [1]. Note that Kloosterman writes in his article that parts of his work are based on gathered knowledge from Laursen and Simo.

3.7.1 Constraints

The impenetrability constrain

In continuum mechanics it is stated, which can be considered self-evident, that two particles cannot occupy the same location in space. For multiple bodies this states that no boundary points between the bodies are allowed to penetrate each other. This reduces the contact problem to a boundary based problem by enforcing that the signed distance of any point on the first body, with respect to the second body, is non-negative. Mathematically this could be enforced with the so-called *impenetrability constraints*:

$$\begin{aligned} d_N &\geq 0, \\ t_N &\leq 0, \\ t_N d_N &= 0, \end{aligned} \tag{3.41}$$

With d_N as the signed minimum normal distance between two body boundaries, the first condition states that no penetration may occur. The second refers to the signed contact normal traction, t_N, and ensures compressive traction. The last condition states that no traction can occur if there is no contact. Of course this also means that if there are no compressive stresses, there is a gap between the bodies.

Frictional constraints

To obtain the effect of friction, the following constraints are taken into consideration,

$$\begin{array}{lcl} \Phi := \|\mathbf{t}_T\| - \mu \|\mathbf{t}_N\| & \leq & 0, \\ \mathbf{v}_T + \xi \mathbf{t}_T & = & 0, \\ \xi & \geq & 0, \\ \Phi \xi & = & 0, \end{array} \tag{3.42}$$

where $\mathbf{t}_T$ is the surface tangential traction vector, Φ states the Coulomb friction condition and μ is the friction factor. Further on $\mathbf{v}_T$ is the slip velocity, which is simply the relative velocity between two points in contact. If the first condition holds, there is no slip between the two points in contact. The second, together with the third condition constrains the tangential traction to work opposite to the slip direction. The last condition states that: There is no slip if the tangential traction has not reached its maximum.

3.7.2 Numerical methods

Equations (3.41-3.42) are the basis of the contact formulation used in finite element calculation. Together with an equilibrium model these equations forms the *strong formulation of contact*. After deriving the strong formulation to its equivalent weak form, one has an equation suitable for implementation into the finite element formulation with the contact normal traction $\mathbf{t}_N$ as the only unknown. However, as this work does not focus primarily on the development of contact conditions, we confine ourselves to that the deriving is in line with the calculation of Equation 3.21. The interested readers are referred to Kloosterman [1].

Most method developed to solve this type of problem are built upon enforcing *equality constraints*, which means that the normal distance has to be exactly zero. As the contact problem is based on an *inequality constraint*, a method has to be developed which choose only those constraints that are active. A constraint is defined as active if it is on its bound when solving the problem. Solving the problem in time increments helps detecting when constraints are switched from being inactive to active. By choosing sufficiently small increments, one ensures that the constraints will not switch uncontrolled during the time step.

An alternative method is to attempt to estimate the value of the normal traction $\mathbf{t}_N$, and thus avoid the explicit active constraint selection problem. In the following approaches the normal traction is interpreted as a Lagrange

multiplier and is assumed to be a function of the value of the signed normal distance.

It can be shown that after deriving the weak form of the contact problem it can be formulated as a optimization problem, where the objective function is subjected to the impenetrability constraint.

$$\begin{array}{ll} \min_f & P(f) \\ s.t. & d_N(f(x)) \geq 0 \end{array} \tag{3.43}$$

The contact simulations done during this dissertation were carried out by two different methods, the *Penalty method* and the *Augmented lagrangian method*, which both make use of this optimization setup. These are two commonly used algorithms which solutions allow a small violation of the constraint in order to estimate the direction and magnitude of the normal traction. The methods themselves are general, and there is plenty of literature on the subject. With reference to the previous reasoning the derivations are not presented, but the methods themselves are briefly discussed.

The Penalty method

The method adds a penalty function to the objective function, containing a penalty term and a measure of the violation of the constraint

$$\min_f \quad P(f) + g(p, d_N) \tag{3.44}$$

where p is the penalty parameter.

Although that Kloosterman[1] implies that the method is easy to implement, it has a built-in disadvantage that the penalty value must be increased to infinity to reach an exact solution. This results in that some matrices get ill-conditioned and discourage a good convergence of the numerical solution. This is a contradiction, and the user has to set the penalty value depending on how important non-penetration is for the application.

The augmented Lagrangian method

By rewriting the minimization problem to a Lagrangian form (still with the use of a penalty factor), one can exploit the fact that the Lagrange multiplier, λ, can be interpreted as the normal traction [1]. A correct estimation of the Lagrange multiplier would yield the exact solution to equation (3.43), however in general one does not know this value. Setting λ to zero the first time and calculate the solution, one obviously obtain a rather poor guess to $\mathbf{t}_N$. But by utilize $\mathbf{t}_N$ as the Lagrange multiplier and calculate a new solution, one will get a better estimate to the result. By doing this iteratively one will obtain a better guess for every time it is done, converging to the exact solution of equation (3.43).

Although this method is more complicated and involves more calculation steps it has some advantages against the penalty method. Since the augmentation of λ helps with the convergence, the penalty parameter can be chosen substantially smaller, reducing the risk of ill-conditioned matrices. This means

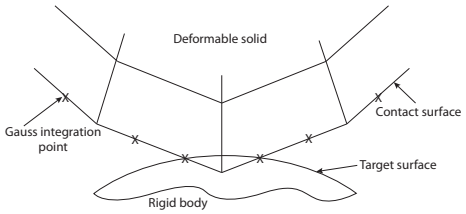

Figure 3.10: Describes how the target and contact surface interact.

that one could get a hold of the actual solution, and still have a stable numerical method to implement. Moreover, it can been shown that increasing the penalty parameter, one gains a superlinear convergence behavior [1].

The ANSYS software has both of the above methods implemented into several elements. The choice of contact element depends on the combination of line to line, surface or point contact. Due to the modeled 3D geometry in this work, the contact always appeared as surface to surface.

ANSYS defines the two surfaces in contact as a target surface and a contact surface, with the restriction that the contact surface are not allowed to penetrate the target surface at its integration points, see figure 3.10.The surfaces that are in contact can be chosen by the user. Then the elements are chosen and positioned on the boundaries where the contact occurs, on top of existing element, automatically by the ANSYS software.

Chapter 4

Experimental tests

This chapter will describe the experimental tests that provide the basis for the second part of the result. First, the choice of test objects is explained, and which properties that had to be taken into consideration for the test. It then describes the test equipment needed, which has been manufactured specifically for this purpose. It concludes with an overview of the tests that have been carried out, and how these have been conducted in detail.

By performing physical tests one illustrates the variations in behavior of the test items that one may not have been able to cover in a prior stage. However, one should be aware that there is always some uncertainty in experimental data, which may be due to several factors such as incorrect sample rate, variations between test items and so on.

The starting point of the test is that, during practically feasible test conditions, perform tests designed to represent the assembly of a heat exchanger. The two main quantities describing this procedure are thus the force the plate package is compressed by, and the permanent deformation the plate package exhibits. By plotting force against deformation continuously during the test one will get a graph showing how plate package stiffness response varies during load.

From a practical point of view it is tedious to deal with full-scale test plates. It is therefore appropriate to try create cut outs from the full-scale plate which are of a manageable size, without sacrificing any response needed during the testing. We have already in chapter 2 given the motivation why to investigate the behavior of the heat transfer surface, and it is this restriction which forms the basis for the upcoming section 4.1. The section after that concerns the clamping tool, which was designed for these tests, and describes its design and functionality.

To be able to compare the test against each other, one must ensure that all testing is done systematically, and thus avoid non-relevant variation between the test objects. In order to achieve this a *Test Specification* was established in advance, describing which test to be done, how they will be carried out and

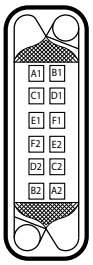

Figure 4.1: Shows the orientation of the plate cut outs of the original plate.

how we determine relevant result. This specification, together with the used equipment calibration records, can be found in Appendix C.1 and D.

In order to control the compression procedure a tensile testing machine was used, which subjected the test items to a compressive load. This type of machine continuously measures the force and displacement that arise during the test. To be able to reproduce the tests or to continue them at a later time, it was important that they were adapted and conducted to Alfa Laval's testing equipment. However, there arose an opportunity in the latter part of the thesis to verify some of the tests on a second test equipment at Lund Institute of Technology. In order to clarify the origin of the data, each test site has been dedicated their own section, later on in this chapter.

4.1 Plates

The test was designed with six plate variants. In order to determine a stiffness behavior for the considered plate model we decided to test all three plate thicknesses, and the two variations of inclination angle (referred as θ_{low} and θ_{high}), that Alfa Laval has in its product portfolio for the intended PHE model. For the tests a total amount of thirty plates were ordered and processed by water jet technique to make sure that the tolerances were met, and that no deformation would occur during the cut out of the plates. From each plate twelve cut outs were made according to a selected pattern, see figure 4.1.

In order to imitate how the cut outs are arranged in a heat exchanger, each plate was assigned an ID A1 - F2, which determines its position on the original plate. Because of that every other plate is rotated 180 degrees during the assembly process, this corresponds to an A1 cut out is stacked with one, 180 degrees turned, A2 cut out. Because of this, it was of high priority to be able to keep track of change for every specimen, as for example their thickness and unique press depth. For this every specimen got an exclusive identification number, which is linked to specimen position letter, the θ-angle, plate thickness and pressing depth. The press depth and thickness for every specimen was measured by hand, both in advance and after the test was performed. Due to the nature of this type of data, it falls within the Alfa Laval's confidentiality agreement and cannot be addressed explicitly in the report. More detailed

information on how this data was measured can be found in Appendix C.1.

Inclination angle consideration

This thesis should provide a foundation for further work at Alfa Laval, which will result in a full-scale model of the whole plate package. With the model as a basis, better estimates of the pressure load against the frame can be made, which in turn leads to an even more optimized frame design. With this in mind, it seems natural that such a modelling approach should focus on the load case that provides the largest stress against frame. In order to design tests that are relevant to this mindset, we need to focus on the plate package which is most rigid, and therefore require the highest load during assembly. Although it is probably rather easy to modify a simulation model that is adapted for a weak plate package, it seems natural that at this early stage start to develop a model that is suitable for the load case which represents a maximum case.

Since we are limited to the cut outs from the heat transfer surface, it is a reasonable assumption that the number of contact points per unit area affects the package stiffness. As the thickness and pressure depht is fixed, the contact point density is controlled mainly by the inclination angle of the plate pattern, see section 2.2. The test plates have two variations of these angles, and therefore, three combinations of contact point density arise depending on whether we combine the $\theta_{high}\theta_{high}$-plates, $\theta_{low}\theta_{low}$-plates or $\theta_{high}\theta_{low}$-plates. By calculating the area for a diamond presented between four contact points, one would obtain an indication of how close these points are located, see figure 4.2. Calculation showed that the combination $\theta_{high}\theta_{low}$ gives the smallest area, i.e provides a denser contact pattern, and the tests should be carried out with this combination.

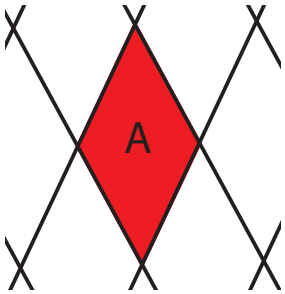

Figure 4.2: The contact density described as a diamond area.

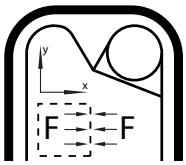

Figure 4.3: The interpretation of boundary condition.

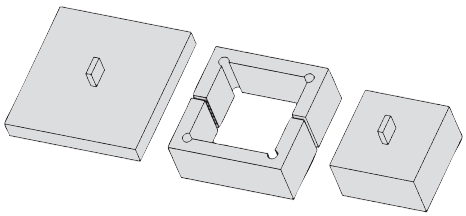

Figure 4.4: The tool parts design

4.2 Fixture

By stacking test items on top of each other in the order described in the previous paragraph, one can reproduce the stiffness contribution from the heating surface in a heat exchanger. To get a result that is representative for a full-scale model, one must take into account that the cut outs are a downscaling of the original plate. We have hence a boundary effect that we have to consider.

With figure 4.2 in mind, consider the same area on an untouched plate that a specific cut out would consist of. During deformation of an untouched plate, the surrounded material will prevent the area element to be extended in the x/y-direction. The chapter on simulation explained that this phenomenon could be modeled by proper selection of symmetry conditions. To achieve the same effect when pressing the test object, its extension in x/y-direction has to be limited. To accomplish this, and to be able to stack the cutouts on top of each other in a stable manner, a tool was developed.

To ensure a reliable functionality of the tool, the needed tool features were set up. These were then reinterpreted into concrete design criteria which served as the basis for the tool design, see Table 4.1. The table describes the desirable feature, which design criteria it results in, whether it is a critical requirement for the tests and finally if the developed design fulfills the criterions.

The final design was made of stainless steel, seen in the figure 4.4, consisting of a pressure tool, a detachable framework and a plan reaction plate. The pressing die and the reaction plate each have a guide rod so they can be mounted in the tensile machine. The frame closes tightly against the plates by pressing the two parts together and removes any glitches with thin pieces of metal, called shims. The blueprints of the design can be seen in Appendix B.1. At the tests performed at LTH, the guide rod had to be removed to fit the equipment, but initially all test was performed at Alfa Laval

Feature to be satisfied		**Design criteria**	**Req.**	**Sat.**
Able to process confined boundary.	→	The tool is able to limit the lateral extension of the cut outs.	Yes	Yes
Able to process unconfined boundary.	→	The solution for boundary expansion and can be temporarily dismounted.	No	Yes
The cut outs shall not extend sideways when using confined boundary.	→	The tools shall be able to adjust so there are no glitch between its walls and the plates.	Yes	Yes
The tool must resist the plates extending force.	→	The tool shall be so stiff that the influence of plate extending force can be ignored.	Yes	Yes
Capacity to stack 16 pcs 0.6mm plate cut outs.	→	Tool size in the height must be at least 40 mm	No	Yes
The reaction support may not affect the plate's deformation.	→	Reaction support and press tools must be flat and able to adjust in position.	Yes	Yes
Tool material must be easily too processed.	→	The tool must be made of aluminum.	No	No
Must fit within the test equipment.	→	The tool is designed with a guide rod.	Yes	Yes

Table 4.1: Interpreted criteria for the tool design process.

4.3 Test performed at Alfa Laval

Most of the tests were done at Alfa Laval. As has been said before, this is due to see if it was possible to conduct reliable tests on the test equipment available at Alfa Laval Lund. There are possibilities to do tests on a more extensive test facility at Alfa Laval in Tumba, but the goal is to run tests locally in order to use the time more efficiently.

Testing was conducted on a mechanical tensile testing machine from Schenck Trebel, with a load cell that is capable of measuring up to 100 kN in force. Due to an uncertainty whether the machine was capable of performing a compression test up to this force, a test was conducted to determine the maximum peak force in both tension as compression. This showed that a compression test could be performed up to 35kN.

The tensile test machine is controlled by software which allows simpler program sequences by defining different blocks, each block defining a specific event of the machine. The program sequence that was used led to that there was an initial force (100 N) applied onto the plates, to ensure that the parts are in contact. The tool is then moved downward at a constant speed of 0.5 mm / min until the maximum peak force of 35 kN is reached. By using a displacement controlled process, one ensures that the plates do not deform uncontrolled. If a load-controlled procedure was used, that is, increasing the load at a constant rate, there could be behaviors that are difficult to measure. One example is that the plates could suddenly collapse at a threshold force.

The software automatically plots the piston displacement relative to the measured force. As a result of the significant strain that the machine is subjected to, the compression of the internal components of the machine will also make a contribution to the measured displacement. As the displacement rate is relatively low, we can manually measure the displacement every ten seconds, and still obtain a good accuracy (see equation 4.1). Even if one measure would occur after eleven seconds, the extra displacement would be negliable.

$$0.5mm/min \Rightarrow 0,0083mm/sec \tag{4.1}$$

Figure 4.5-4.6 shows the test equipment when it is setup and a cross section where the test plates can be seen. The picture does not show the shims which have been used to prevent clearances between the tool frame and the plates. To ensure that the framework is not extended during the tests, we used a clamp to hold together its two parts. Measurements were made with a dial indicator with its measuring tip set on top of the press tool. After the machine had imposed its initial pressure, the dial indicator was reset before continuing the displacement. After every ten seconds the current compression force was noted in a test protocol.

Table 4.2 illustrates the tests that have been done at Alfa Laval. Each test was meant to be carried out three times to give a mean result. Test variety was selected to reflect the differences between plate thicknesses, but also behavior differences between different numbers of plates.

Tests carried out with two plates, to confirm which combination of inclination

		Plate thickness			Notes
		0.4	0.5	0.6	
No. of plates	1	•	•	•	—
	4	•			Also done w/o boundary frame.
	8	•	•	•	—
	16	•			—

Table 4.2: Test done at Alfa Laval

		Plate thickness			Notes
		0.4	0.5	0.6	
No. of plates	1	•			Also done w/o boundary frame.
	8		•	•	—

Table 4.3: Test done at LTH

angles who gives the stiffest response, have been chosen to be excluded. This due to the impact by the tolerances, and the differences in number of contact points, was considered too large for the result being useful for further analysis.

4.4 Test performed at LTH

Lund Institute of Technology was in latter part of the project providing a hydraulic test machine, which compressive force was so large that in practice there was no limit for our test. There was also made a calibration sample, which means that the machine's self-compression can be subtracted from the test data. This gave us an opportunity to use the machine's own measuring equipment to plot the force and displacement. This results in higher measurement accuracy and sampling rate. The tests that was conducted can be seen in Table 4.3.

Figure 4.5: The setup of the tensile test. In front one sees the dial that measures the displacement.

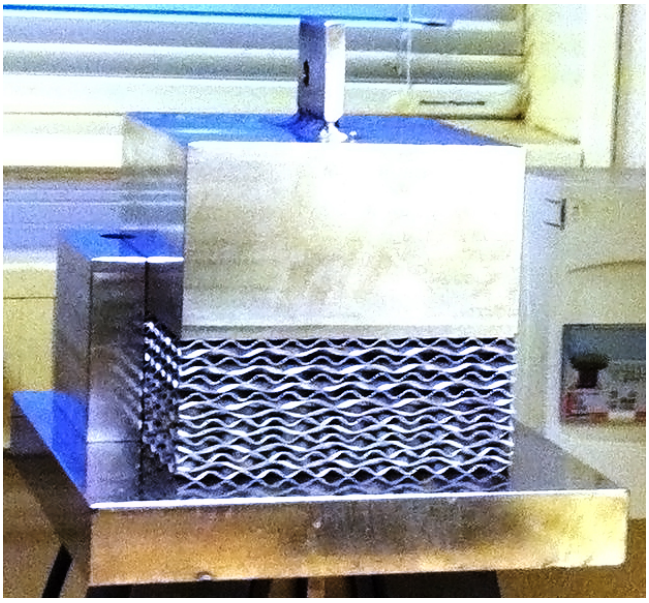

Figure 4.6: A cross section which shows how the plates are stacked

Chapter 5

Simulation

In this chapter the method for the performed simulations is presented. The process starts from the basic idea for the simulation and ends up with the tested models. The results from these simulations are later presented in chapter 6.2. Even models that did not succeeded in a proper result are considered.

All simulations where performed in ANSYS Workbench 12 which is an engineering simulation software for these kind of problems. The component used in this software is the ANSYS Mechanical. CAD modelling parts for the simulations were created in Autodesk Inventor.

5.1 General approach

The purpose of the simulation tests was to achieve a model that could verify the experimental tests. This because of the great gain of time and resources in further development of new products. How complex the model for these simulations should be was depending on the outcome from the experimental tests. The limit for this complexity is to find the satisfying relation.

The initial starting point for the simulations was a basic idea of how this should be completed, see figure 5.1. This idea was to simulate the pressing of a plate followed by a compression of the pressed plate. During the compression the forces and the corresponding displacement should be identified and plotted. This relation will in other words be the stiffness for the plate. If the simulation should be in two dimensions or if a three-dimensional analysis was necessary was initially unknown.

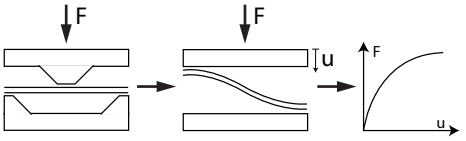

Figure 5.1: Chain of events during simulations

When investigating this problem it turns out to be a coupled problem with two

individual problems from a simulation point of view. In the first simulation a forming tool is needed to create the shape of the plate. Further on one have to release the now pressed plate from the forming tool and compress it between two plane supports. For this type of analysis ANSYS Workbench delivers two possible ways of doing this.

The first is to separate the two problems and have the residual stresses and the deformed geometry transferred from the first to the second problem. The command taking care of this is the *INISTATE* command. Basically this includes a write-command saving the data from an analysis and one read-command loading this data into a new analysis. To get this working properly the mapping between the configurations is very critically. One has to secure that the numbering and the position of the elements is exactly the same in the both analysis to have a satisfying result. Some simulations in this project where tried with this INISTATE method but the mapping did not satisfy our needs and further investigations where not possible cause to lack of time.

The second way to solve the problem is to perform a multi-step analysis. This is also the procedure that the simulated tests for this project are based on. This is mainly one analysis with a number of time steps. The major challenge for this setup is to get the correct contact switches during and between the time steps. E.g. when the plate is pressed by the first pressing tool and this tool is released the contact should be overtaken by the plane supports. If a non-correct switch is done the numerical solution may have convergence problem. The simplest way to avoid this phenomenon is to insert fixated nodes that prevents rigid body motion. One has to be cautious that these points do not affect the result.

Another aspect of this procedure is that to get the right contact switch you have to know how the pressing for example makes the plate thinner in some areas. If the initial geometry then is changed, another setup for the contact switch have to be taken into consideration. The following sections present the setup for the simulations.

5.2 2D Analysis - Flank model

The first setup for the problem was in a two dimensional manner. The major benefit of keeping simulations in 2D is that the simulation time is very short and the required computer power is low. The consequence of this is that the contacts appearing when one have a stack of plates is impossible to simulate. Thereby these simulations were made according to the experimental single plate tests, see sections 4.3-4.4.

This was also made in a second version where the plate was imported to the analysis as already pressed. The consequence of this is a plate that initially is without any residual stresses, plastic deformations and thinning effects.

The model simulates a plate with a thickness of 0.4 millimeters. Symmetry was added as fix boundaries in x-direction and the displacement of the supports, affecting the plate, is applied as seen in figure 5.3.

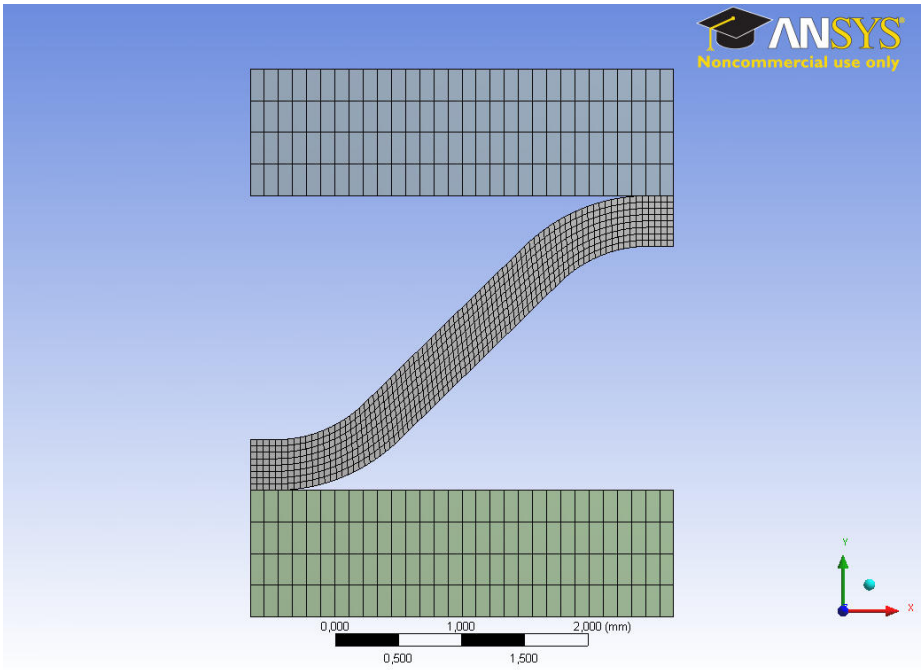

Figure 5.2: The element mesh for the 2D flank simulation

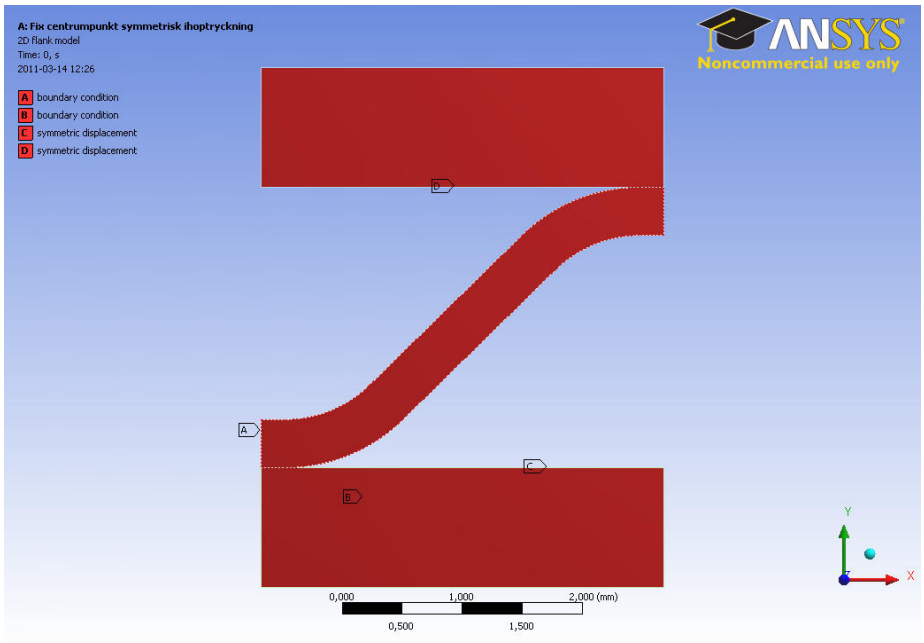

Figure 5.3: The setup for the 2D flank simulation run

5.3 3D Analysis - Rhomb model

To try to show the behavior when two plates get in contact with each other and local deformations occur, a setup with a 3D model with the geometry of a rhomb was simulated. The contact angle for this rhomb section was according to the θ_{high} as a first step to see how the outcome was. As seen in figure 5.5 this setup was made without initial stresses and plastic deformations.

The number of flanks or contact points were varied from 1-16 for this analysis to see if the boundary affected the result. Each test was increased with one plate, until a test with four plates was reached. The table below, see Table 5.1 denotes the test matrix.

		No. of contact points						
		1	2	3	4	6	9	16
No. of plates	2	•	•	•	•	•	•	•
	3	•	•	•	•	•		
	4	•	•					

Table 5.1: The test variety for the 3D rhomb simulation

The model is with the plate thickness of 0.4 millimeters. Boundaries were fixed in the normal direction to each surface and the displacement of the supports affecting the plate is applied as seen in figure 5.5.

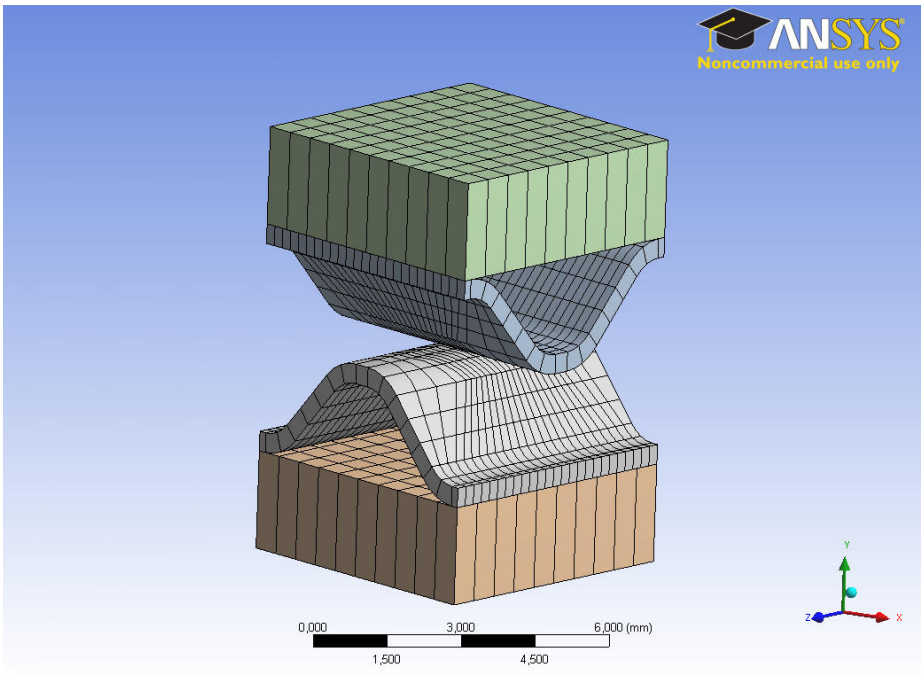

Figure 5.4: The element mesh for the 3D rhomb simulation

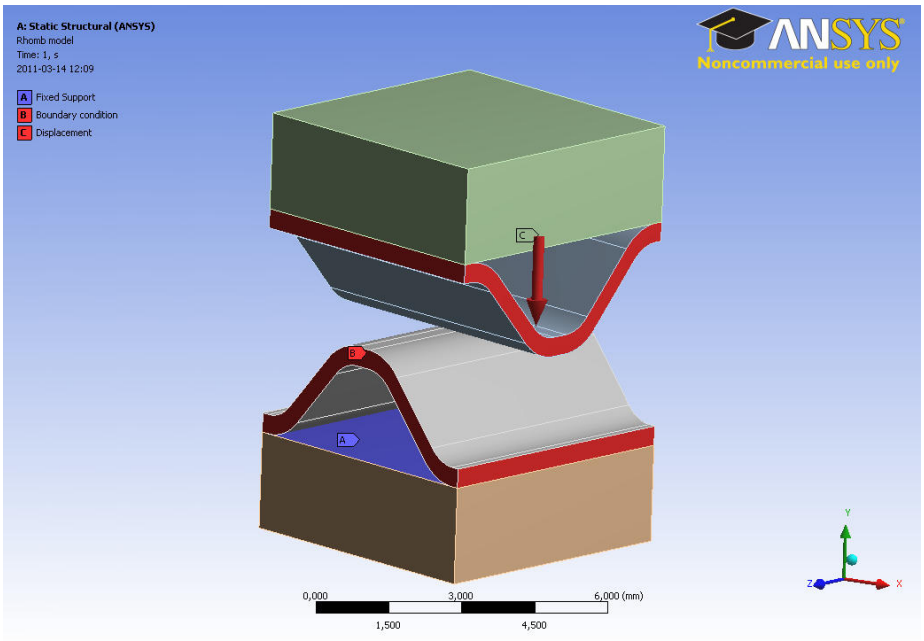

Figure 5.5: The setup for the 3D rhomb simulation run

5.4 3D Analysis - Rectangular model

The last model tested was a thee-dimensional rectangular model with two plates. It was tested to get the correct contact between the plates and to include residual stresses and plastic deformations from the pressing. The setup was much like the initial idea with the multi step analysis, see figure 5.6-5.7.

With help of simulated dies, two 0.4mm plate is first pressed to their final geometry. In the second step the dies are removed and the two plates are pushed together and thus forming mechanical contact between them.

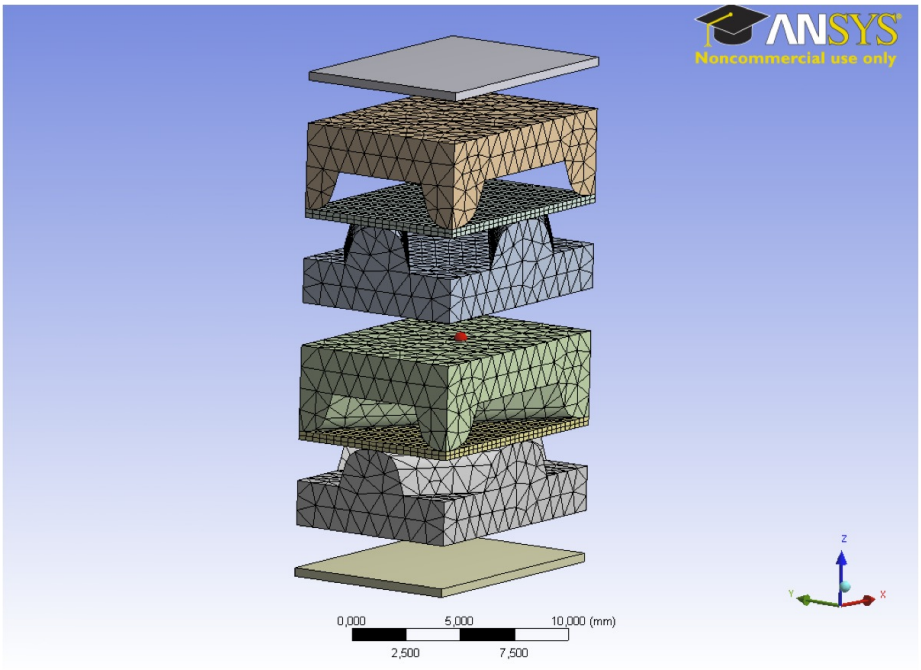

Figure 5.6: The element mesh for the 3D rectangular simulation

A rectangular section has the advantage that the boundary surfaces of the model are orthogonal to each other. Since the chevron pattern is geometrically repeatable this also gives the possibility to use what is called *periodic symmetry*. This periodic symmetry condition relates the boundaries so that the motion for one boundary surface with the normal x_i-direction moves exactly like the other boundary surface with the same normal direction. Implementing this to the analysis is made by the command CPCYC. The CP commands refers to a type of commands coupling two nodes to each other and the specified CYC is suitable for cyclic setups. When having a two-dimensional symmetry like this one has to use the command twice to couple each direction. Since a coupling between two nodes links every degree of freedom of them, one has to treat the corners separately to avoid conflicts or as to say double couplings. A double coupling is when the degree of freedom for one node, like a corner node, is coupled to two

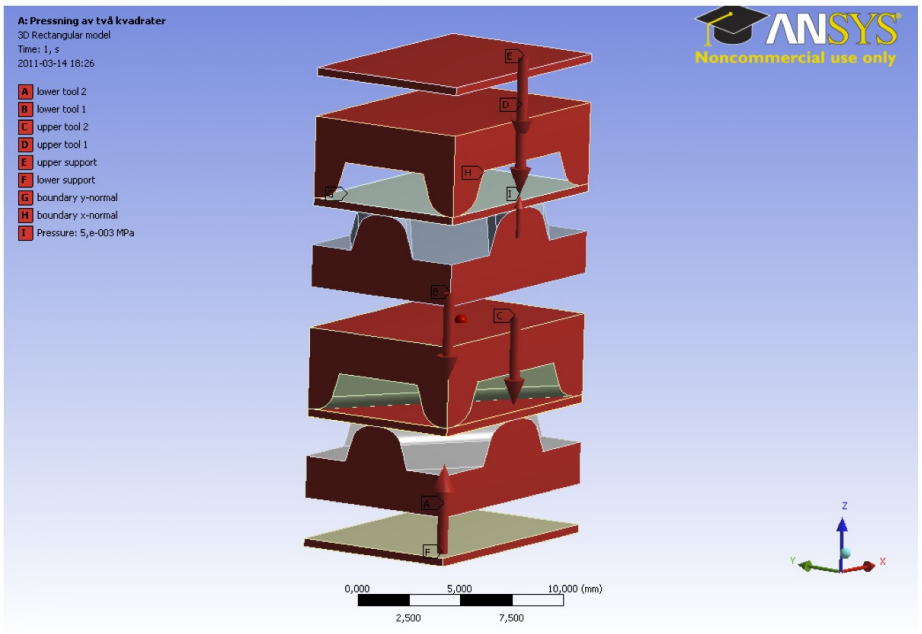

Figure 5.7: The setup for the 3D rectangular simulation run

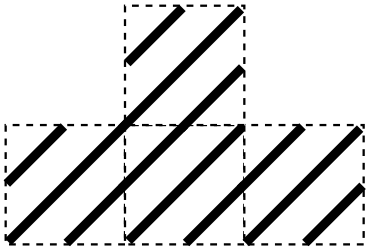

Figure 5.8: The theory for periodic symmetry

other nodes, the both corresponding nodes in each normal direction. This leads to a conflict.

One should note that cyclic couplings require identical node and element patterns on the corresponding surface boundaries to get proper couplings.

Unfortunately for this master thesis there was no satisfying solution with the periodic symmetry implemented. This because of lack of time and contact switch problems that is prior discussed. The deformation appears differently when introducing periodic symmetry that gave contact difficulties. A successful result is shown in the result chapter where the simulation is solved without the periodic symmetry condition. This result shows the impact of the periodic symmetry conditions or more the absence of it.

Chapter 6

Result

In this chapter the results from the experiments and simulations are presented. At first one should see these two parts as separate presentations. In chapter 7 the results are discussed and related to each other to find similarities and differences. The test methods behind these results were described in chapter 4 and chapter 5.

6.1 Experimental test result

The sampling at LTH was carried out electronically, which led to a considerably higher resolution of the collected data. Small changes in the measurement signal are reflected in the data, and appears as small deviations from the graph trend line. This is why the graphs from the LTH tests can appear jagged, in comparison with the Alfa Laval tests.

In order to compare different tests with each other, the graphs are scaled to the number of plates in the tests. If a test was performed with eight plates stacked on top of each other, the displacement has been divided by eight to illustrate the mean plate deformation.

Due to the cut outs were not perfectly flat, the whole plate package will not come in contact simultaneously. This gives rise to different initial behavior of the various tests, and it had to be assumed that at a certain force all the plates was in initial contact. The zero displacement for the actual test is related to this force.

Another relationship is then used to compare the tests. This relationship is based on plate tolerance on thickness and pressure depth. The zero value on the displacement axis corresponds to a plate with nominal dimensions. A plate with nominal tolerances is compressed $0.03mm$ to reach the assembly length, marked in the graphs with a dashed line as *A-length*. A plate with positive tolerances has to be more compressed to reach the same assembly length and thereby it will be moved to the left on the displacement axis.

The tolerances for each specimen are displayed in the graphs. The notation

for this is

$$p : 0.0xx \; t : 0.0xx \tag{6.1}$$

Where the p : is the actual pressing depth tolerance and t : is the thickness tolerance in millimeters. This tolerance can be both positive and negative values.

6.1.1 The collapsed plate and boundary behavior

The graph in figure 6.1 shows the behavior for a plate when it is pressed until it is flattened. The collapse test was done without any boundary box due to the large expansion of the plate. The second curve corresponds to a test with the boundary box, which clearly shows that this box prevents the plate from collapsing. The behavior at lower loading levels is however very similar even if the test without boundary box shows a slightly softer plate behavior. The

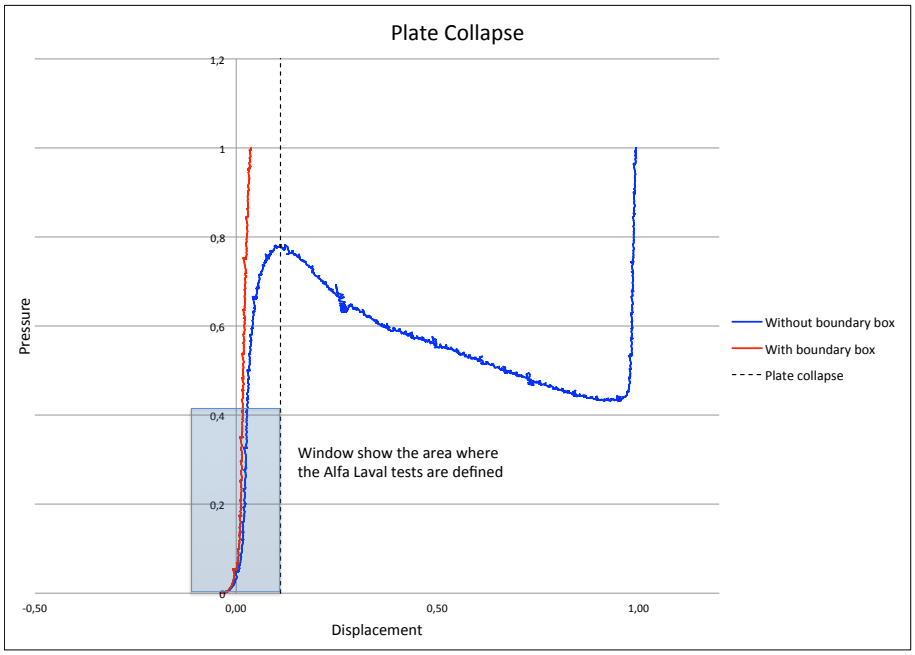

Figure 6.1: The behavior of a plate that is pressed until it is flattened.

highlighted box indicates the area where the Alfa Laval tests ranges within. This force/displacement range may look insufficient but it covers all relevant cases that occur during assembling a plate heat exchanger. In reality the plates are never exposed to loads that could flatten them. In figure 6.2 the graph shows the highlighted box more close up. As said in the beginning of this chapter, the LTH tests can appear jagged due to sample frequency.

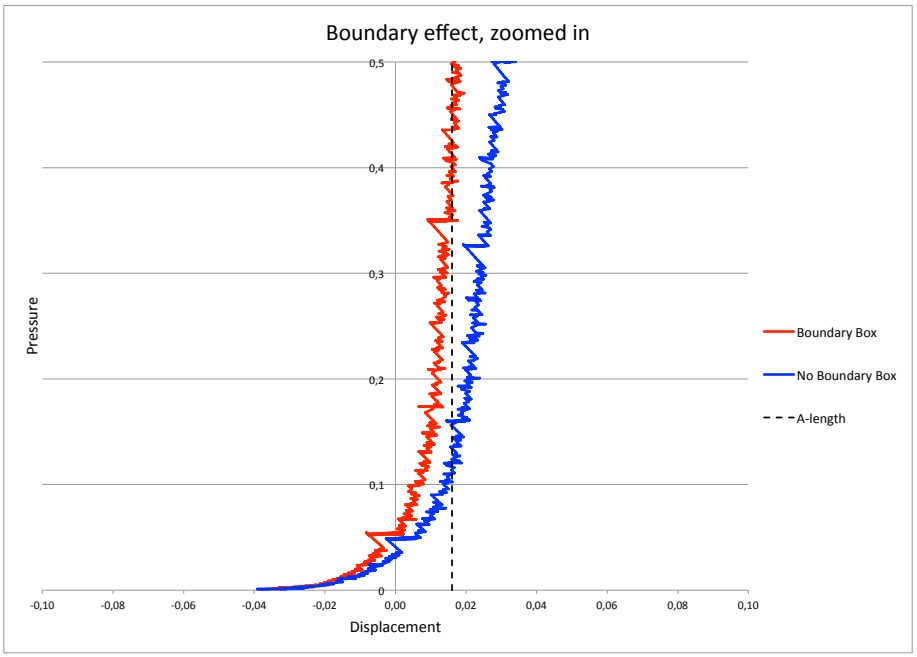

Figure 6.2: Shows Figure 6.1 zoomed in at the highlighted area. Tests conducted at LTH.

Boundary effects

Figure 6.3 shows the influence when tests are made with or without the boundary box. The test consisted of four 0.4mm plates, where the graph has been scaled to show the behavior of one plate.

A boundary plate is defined as the one closest to the dies, which leads to a unique contact situation compared to the plates stacked between them. Due to the chevron pattern, the die comes in contact with several ridges on the plate. Compared to a plate-to-plate contact, which forms an point contact, the ridges-to-die forms line contacts all over the plate. This results in a substantially larger contact area compared with the area between two interacting plates.

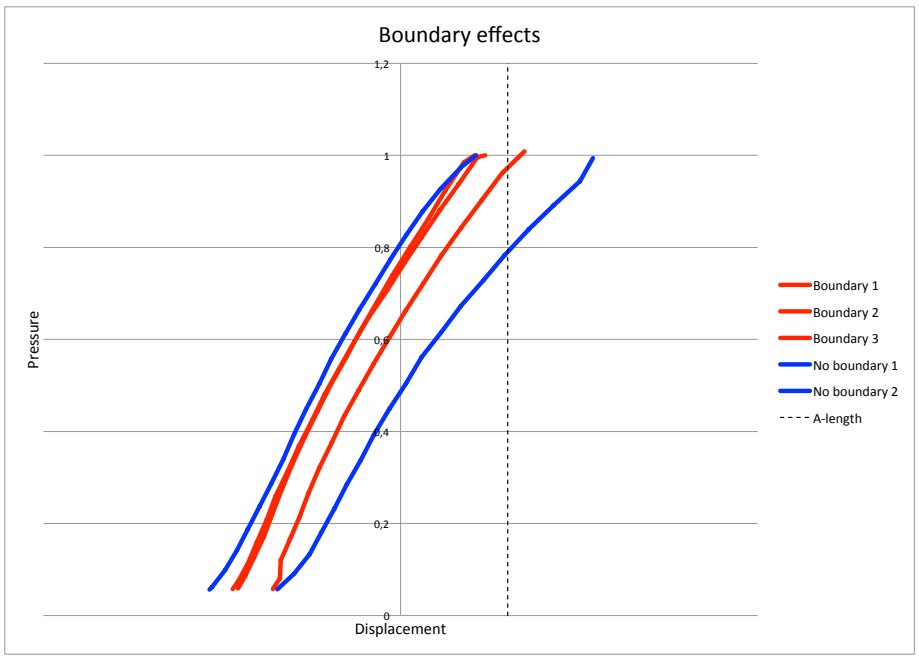

Figure 6.3: The influence of the boundary restriction during a compression test, conducted at Alfa Laval.

6.1.2 Single plate tests

For the tests where one plate is compressed the only contact occurring is against the upper and lower dies, and both sides of the plate forms the same contact as a boundary plate. This contact along the flanks prevents local point deformations from occurring, as it would if it was a plate-to-plate contact. The deformation for these tests is thereby only from global deformation of the corrugated pattern. In other words this means that all deformation is due to that the corrugated pattern is flatten out. In figure 6.4-6.6 the result for 0.4/0.5/0.6 mm single plate test, are shown.

In figure 6.7 one plate of each thickness is shown for comparison. Some of the following curves are not moved along the x-axis as the other graphs. This is because the graph is meant to show the stiffness differences between the plates, rather than tolerance differences.

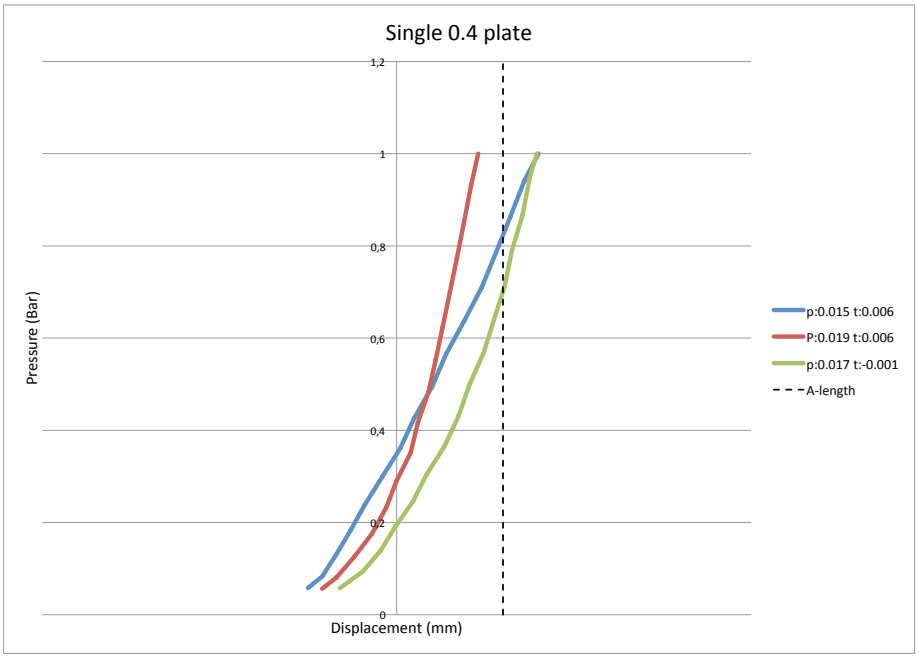

Figure 6.4: Single plate 0.4mm conducted at Alfa Laval.

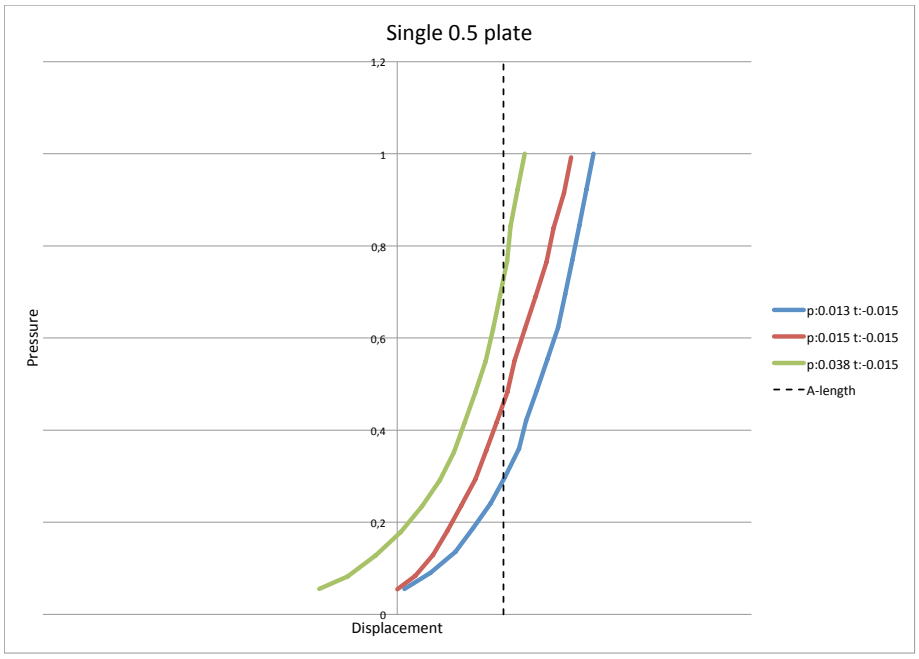

Figure 6.5: Single plate 0.5mm conducted at Alfa Laval.

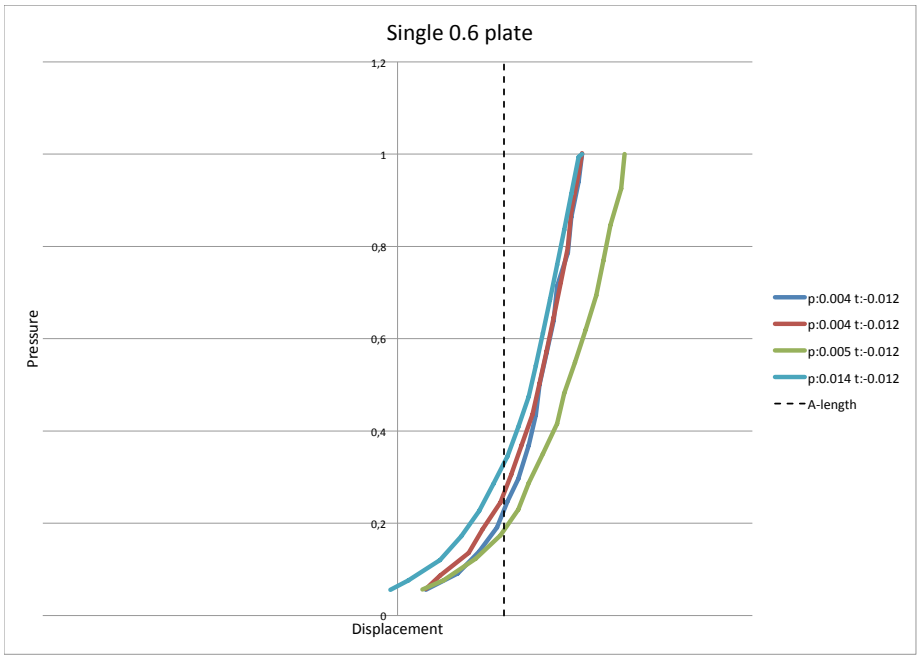

Figure 6.6: Single plate 0.6mm conducted at Alfa Laval.

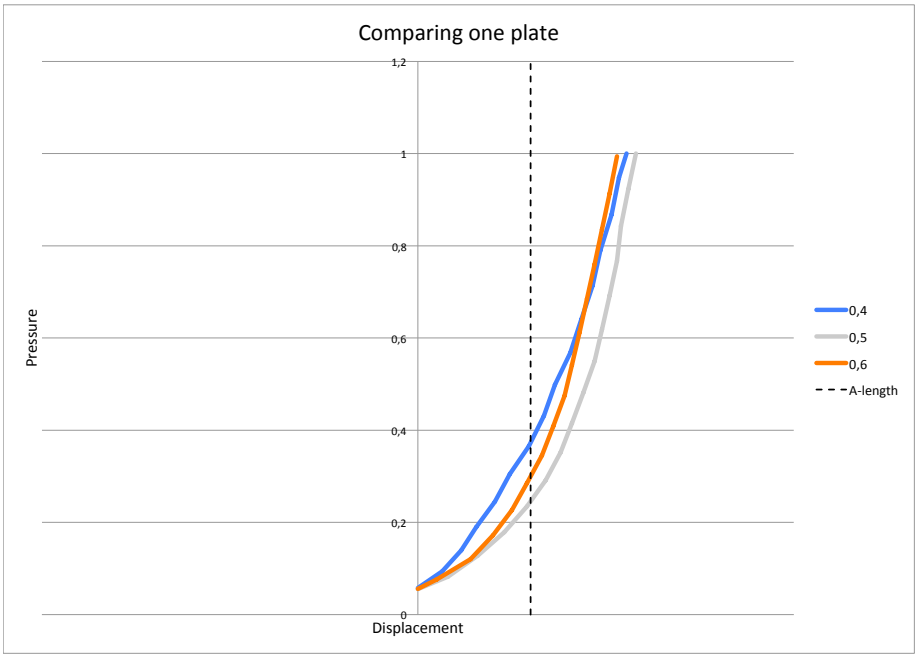

Figure 6.7: Comparison between single plate tests, conducted at Alfa Laval.

6.1.3 Multiple plate test

The first graph, figure 6.8, consist of only 0.4 mm plates and shows the behavior when the number of plates, stacked on top of each other, are changed. The curves are color grouped accordingly to the number of plates used. Figure 6.9 shows the same result as 6.8 but scaled according to the number of plates in the test.

The figure 6.10, shows the behavior when one varies the plate thicknesses. Each test has a number of eight plates stacked. Due to a more powerful test equipment at LTH, these test has a higher load range. The next graph, figure 6.11, displays one plate thickness each of the figure 6.10 graph. These three graphs are considered to represent a good average of its own plate thickness and are assumed to be a nominal plate in the following graphs. Figure 6.12 shows an example of the trend stiffness where linear trend lines of the curve is added in three parallel moved versions. This corresponds to diffenrent tolerances values of a plate and displays the influence of this tolerance. This type of graphs shows the pressure range which the plate package are exposed to when compressed to the nominal a-length, corresponding to a specific plate tolerance.

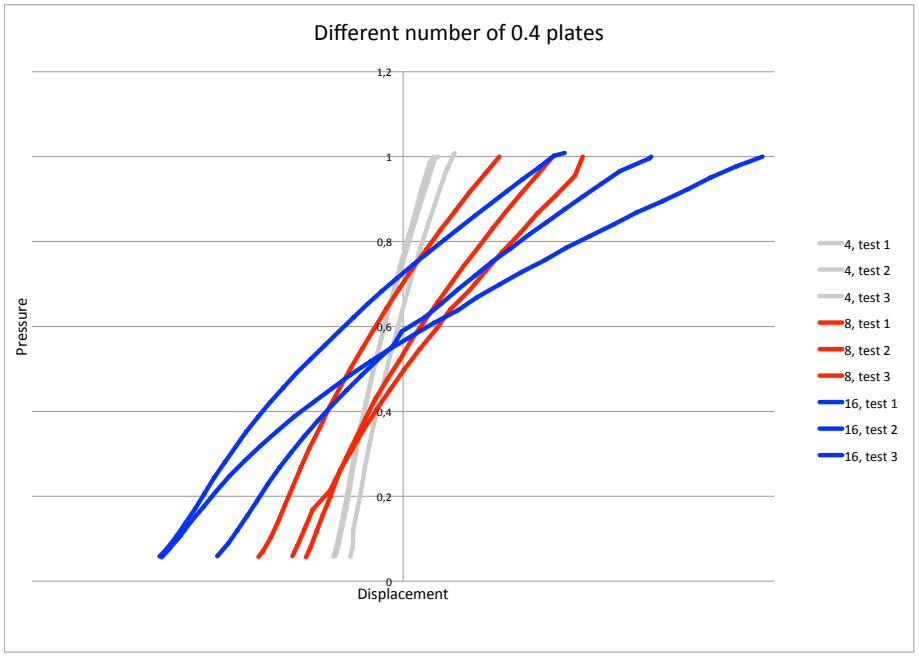

Figure 6.8: 4, 8 and 16 plates, 0.4mm, conducted at Alfa Laval

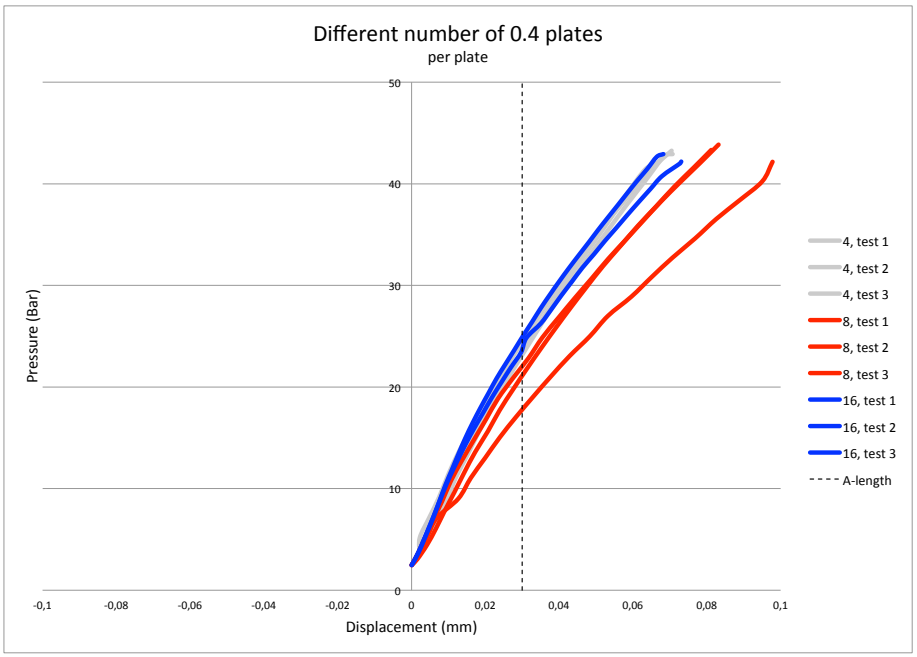

Figure 6.9: The stiffness according to number of plates, conducted at Alfa Laval.

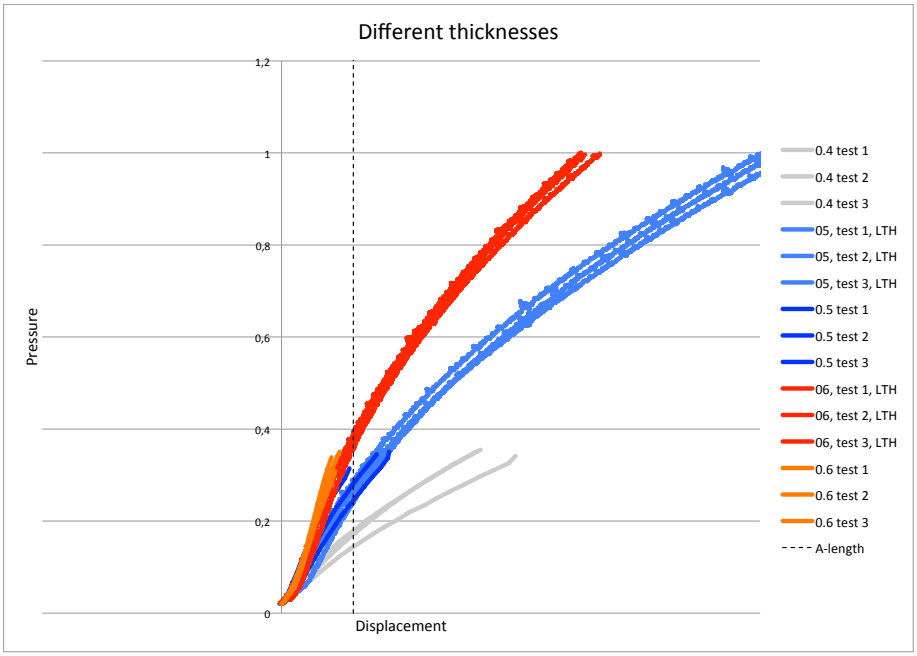

Figure 6.10: 0.4, 0.5, 0.6mm plates.

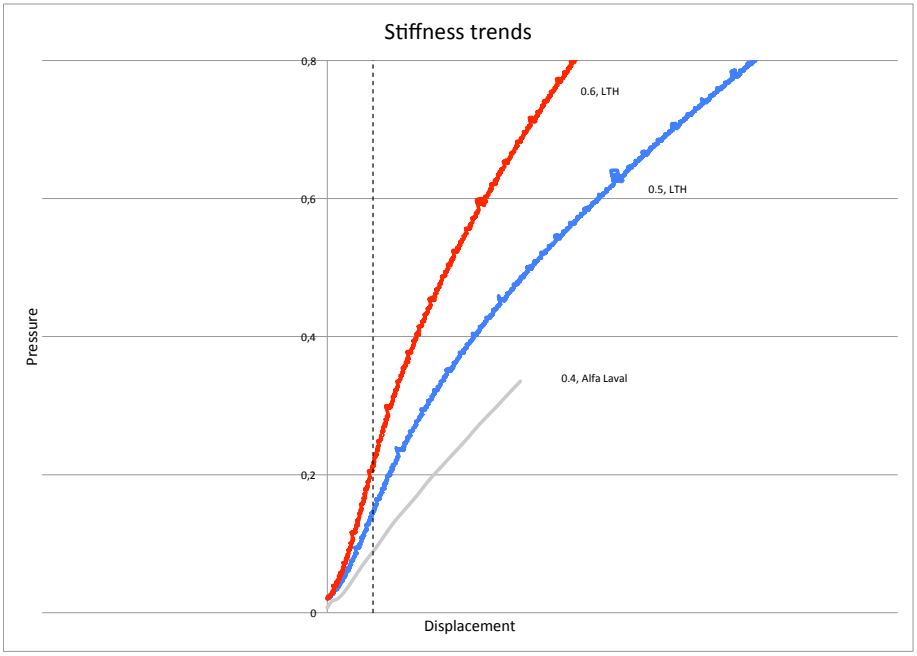

Figure 6.11: Trend stiffnesses for different thicknesses.

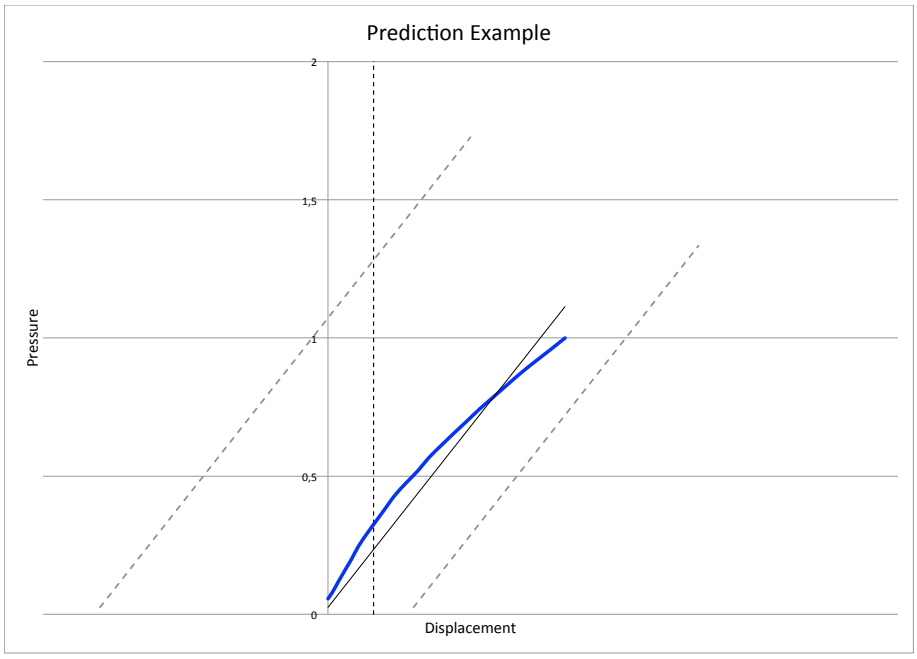

Figure 6.12: Trend stiffness example according to tolerance.

6.2 Simulation result

This section shows results for the two simulation models flank and rhomb. The results show the difficulties and assumption which are overcome on during the process.

6.2.1 2D Analysis - flank model

Figure 6.13 shows a simple simulation of the flank model, without any residual stresses and strain. Due to rigid body motion the simulation was aborted, and a fixed node was introduced at the center of the plate to handle the problem. Figure 6.14 shows the stiffness variation of the flank model when it is simulated without any residual stresses and initial plastic deformation. In the same graph, a solution with residual stresses and strains is also shown.

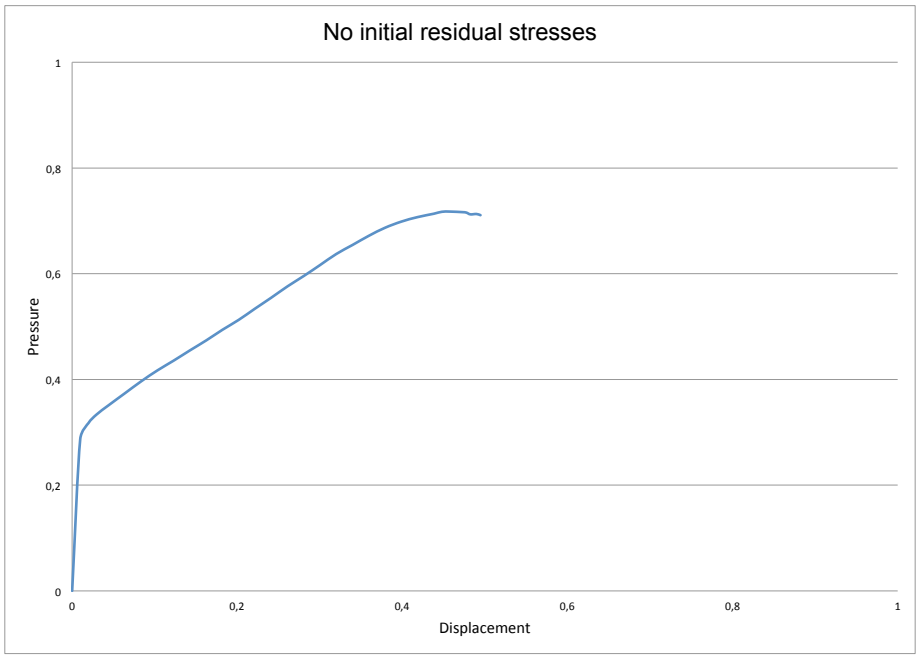

Figure 6.13: 2D flank simulation *without* a fix center nodal point.

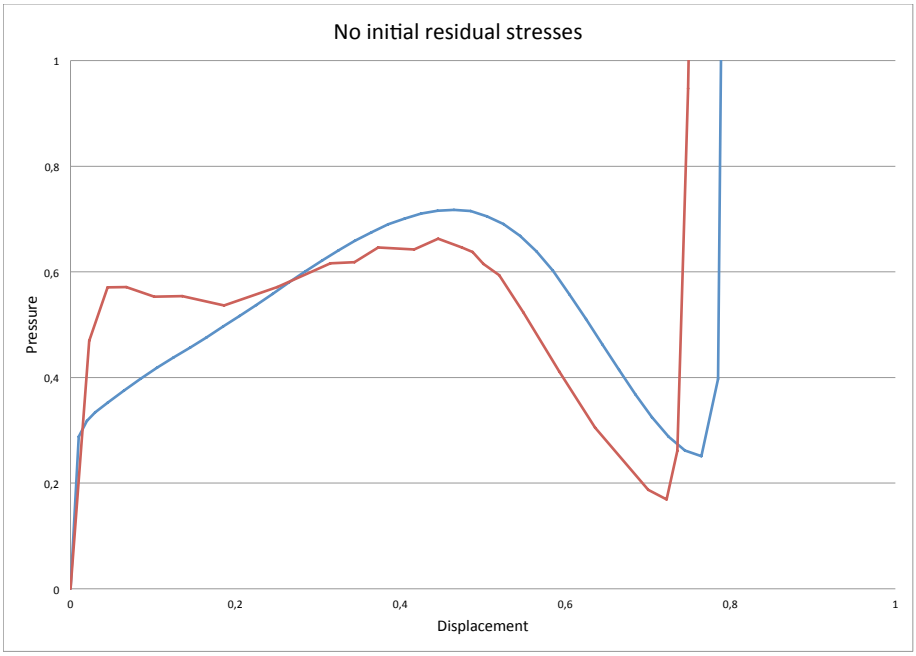

Figure 6.14: 2D flank simulation with a fix center nodal point.

6.2.2 3D Analysis - Rhomb model

Figure 6.15 shows the stiffnesses for the rhomb model simulations. The results shows small variations between the tests, but the highlighted line represent the median curve. The graph legends are sorted in a descending order according to plate stiffness in the graph. The result shows that this order coincides with the number of plates, where fewer plates shows a stiffer response. Even though, there is some anomalies.

As all simulated plates has a nominal thickness and press depth, there are no repositioning along the x-axis of the curves.

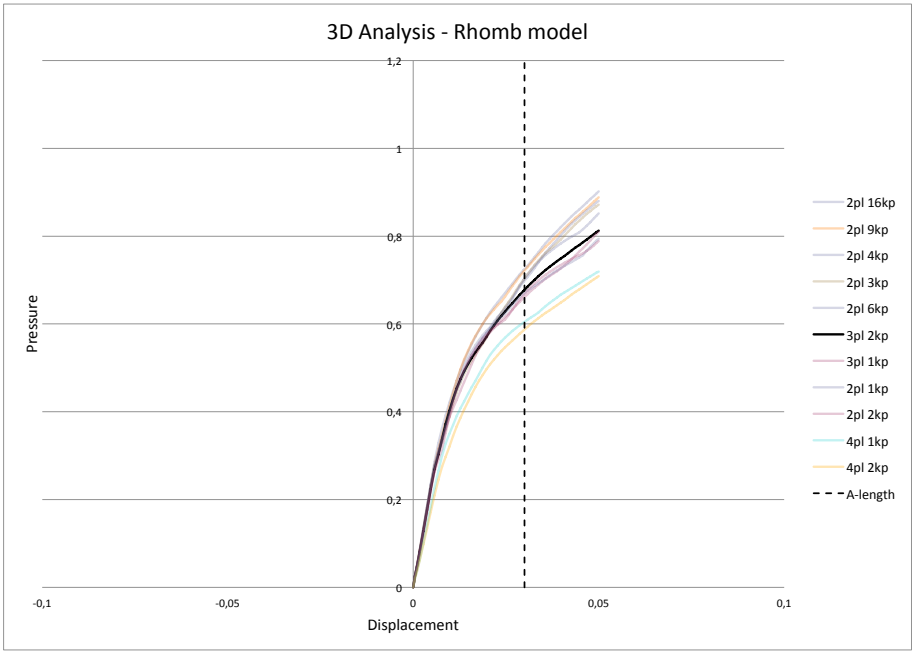

Figure 6.15: 3D rhomb simulation of 0.4mm, which shows all test specified in section 5.3

6.2.3 3D Analysis - Rectangular model

Figure 6.16 shows the deformed rectangular simulation, where two plates were pressed together. The simulation covers the entire sequences from that the plates are pressed into the right pattern, until the plates have been pressed together with each other and formed mechanical contact. This means that the simulation takes residual stresses and plastic strains into consideration during the run.

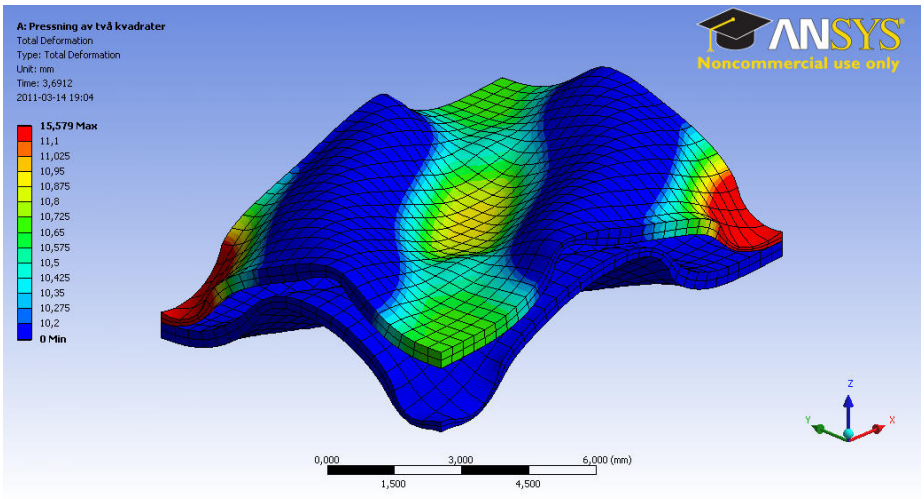

Figure 6.16: 3D Rectangular simulation without periodic symmetry. Note the contact points forming in the middle.

Chapter 7

Discussion

This last chapter summarizes and discusses the results from both the experimental tests and the simulations. Problems and difficulties encountered during this master thesis project are briefly considered at the end. Finally, we present our thoughts on how further work should be planned, what aspects to consider and what one should put extra emphasis on.

7.1 Experimental test

7.1.1 The collapsed plate and boundary behavior

The plate collapse test, see figure 6.1, gives a clear picture of the overall collapse appearing for a plate like this. Initially the plate performs very stiff when pressed together whether a boundary box is used or not. The maximum sustainable load is reached when the plate is pressed together about $0,2$ millimeters. This for the plate without any boundary limitation. After this peak the response is a weaker stiffness until the whole pressing depth is reached. It is realistic to consider that the behavior is related to a "snap-through" behavior. By this means that the stiffness of the plate abruptly breaks and flattening of the plate occurs. If ones test instead of being controlled by displacement is controlled by increasing force then this behavior cannot be simulated.

The test with the boundary box, figure 6.2, obviously does not collapse like the other one. This must be because of the boundary box. In other words, the plate appears more rigid with this limitation due to restricted internal displacement of the plates. It can also be assumed that a boundary box gives a slightly stiffer overall behavior in relation to the test without boundary box. For these one-plate tests there are a significant difference between the tests. This influence of the boundary box is however hard to estimate in figure 6.3. This figure shows no remarkable difference between the tests.

The explanation for this may be because of the contact points. When pressing just one plate the contacts are against the pressing dies. This contact area is along the top of the pattern and is much larger compared to the contact area

found between plates where initially only point contacts occur. Thereby one can assume that when tests are done with stacked plates the response will be softer. Due to local deformation points the plates will in some way act like springs introducing flexibility to the package. The displacement of the package will also be more controlled by the contact points than of total plate deformation. This flexibility is thereby assumed to reduce the influence of the boundary box.

Since the tests are made on small specimens according to the total plate one can discuss what kind of tests that are most similar to the real plate assembling. In reality there is no restricting boundary box enclosing the plate but on other hand there is surrounding material preventing this material movement. The answer should be somewhere in between. A boundary box for these small specimens result in a too stiff material and a test without this boundary box will be softer than the real plate.

7.1.2 Single plate tests

The single plate tests confirm the previous discussion on the plate behavior. Even if the range of the single plate tests not dot reach the collapse load, the conduct of this tests is very similar to the plate collapse test. Remarkable is the comparison of the different thicknesses, see figure 6.7 where the difference of displacement according to thickness seems to be very small. The absence of local contact deformation points for these tests result in that the plates appear approximately equally stiff independently of thickness. It is thereby the plate pattern, or so to speak, the corrugation that sets the stiffness of one plate.

7.1.3 Multiple plate tests

Introducing local contact points will change the reasoning that the different plates will be equally rigid. Figure 6.8-6.10 provides another view of these different stiffnesses and in contrast to the tests with one plate, this show a totally different stiffness according to thickness and number of plates. The tests with different number of plates shows the impact of this number. As expected, and as, seen in figure 6.8, one is capable of compressing a package with an increased number of plates further than a package with fewer plates. Since the range of number of plates for the tests is limited its hard to conclude anything about how this relation is when a large number of plates is used. Due to figure 6.9 there is a slight variation of stiffness,with increasing stiffness for $4, 16$ and 8 plates. This difference must be due to the development of contact points. It indicates that a thinner plate is more sensitive to local deformations and thereby gets a lower stiffness. Though, the resolution of this change in stiffness is not sufficiently large enough to detect a softer behavior using only the tolerance value of the plate thickness because of the small percentage this tolerance represents. The fact that the LTH tests show a very similar relation also strengthens these conclusions.

When transforming these stiffnesses into trends for each plate type, see figure 6.11, one get a clear picture of how great the range is according to the plate

tolerance. For example, $0.6mm$ plates with a high tolerance will cause a very high stiffness.

One may assume that plates with position closest to the dies for each test will appear stiffer because of the increased contact area. These boundary plates will have less influence to the total compression of a package when the number of plates is increased. With this reasoning, more plates should give a softer response. Although this conclusion seems logical, the result in figure 6.11 do not follow this reasoning. This may be due to uncertainty in the test as a result of such tolerance deviations, too few tests or too few combinations of number plates. There is a possibility that the argument is strengthened when more test sessions is done with a broader range of number plates.

7.2 Simulation

7.2.1 2D Analysis - flank model

This simulation shows clearly the importance of a fix reference point for a simulation to avoid convergence problems. The non completed simulation, 6.13 is a typical example of this where the numerical solution is in need of a fixed point. The impact of including residual stresses and initial plastic deformation, see figure 6.14, seems only to contribute a minor effect in the range which is in interrest for Alfa Laval.

When trying to associate this simulation to the experimental results the similarities are hard to find. The corresponding experimental test would be the collapsed plate test. Even if the overall curvature got some similarities with this test the deviations prevent any real comparison. The model is considered to be of subordinate importance for modeling the assembling scenario.

7.2.2 3D Analysis - Rhomb model

Further on analyzing the rhomb model result with the response seen in figure 6.15. The corresponding experimental test to this simulation should be the 6.8 where the thickness is constant and the number of plates is varied. The general behavior is rather similar with an initial stiff response that becomes slightly softer when increasing the displacement. The model got more of this effect than the experimental test and if the differences between the simulation and the test are considered this seams to be predictable. First of all, the simulation model is based on a very small area compared to the experimental test. When having a smaller area the boundary effect will have a higher percentage impact and thereby an increased influence on the result. The absence of initial plastic deformations will in other hand contribute to a softer behavior, this since the plastic deformation increasing the stiffness to the plate design. In the same manner as the experimental collapsed test loose the initial stiffness when the top of the pattern breaks, the model perform softer when the contact point start deforming the top of the pattern.

Even if this model do not corresponds exactly to the experimental tests it gives at least some indication of how a more accurate model could be designed.

7.2.3 3D Analysis - Rectangular model

The purpose of viewing the results from this simulation, even though it was not completed, was to elucidate the effect of insufficient symmetry conditions. As seen in figure 6.16 the plates are not deformed symmetric. The lack of periodic symmetry conditions allows the boundary edges to deform unequally. Utilization of correct conditions would force the two front corners to deflect the same amount. Instead, the left and right corner are weaker than they should as the underlying plate do not give the same support as it is expected to do in a real application. As told before there are ways to introduce that kind of symmetry in Workbench, but it has to be done by scripting and is not user friendly. ANSYS Workbench is marketed as being an easy to use program with features that has graphical interfaces, thus it is reasonable to assume that it is addressed to a user who is not accustomed with ANSYS scripting language. That together with the difficulty to diagnose why the simulation does not converge, and how much of the problem that is connected to the symmetry condition, makes us think that the software in the current version does not provide a sufficiently user-friendly method to solve this type of problems.

7.3 Conclusions

Since the purpose of the experimental test was originally to be able to prove a simulated model they were made in a limited number. A more detailed understanding of the influence from the differing press depth and thicknesses according to tolerances is very depending on this spectrum of testing and could not be investigated as desired. To get a more detailed understanding of the influence from press depth and plate thickness on the stiffness behavior, we would need to have a lot more test objects with varying tolerances. From the relative small amount of test that we had time to conduct, it is hard to give any reliable conclusions of how the stiffness response would be of a hypothetical plate with a defined tolerances. However, one can identify trends in the plate's behavior which can then serve as a basis for future assumptions about the needed compression force.

Although the experimental tests gave a good picture of how the plates appear during compression at a general level. One should be aware of that the tests only took place in the range of 4-16 plates and therefore assumptions that are made outside this range should be made with caution. Even though some GPHE's do ship with that low amount of plates, they can also come in versions with over several hundred plates.

The trend curves also provide the large range of pressures that can be required with respect to the plate tolerances to reach the nominal assembly length. The fact that this assembly length for the tests is set with a relation to a given

force gives an uncertainty of the exact position of this length. Thereby one has to take this into consideration when discussing correct pressure levels. It is obvious that a small error in position of the nominal assembly length result in a sufficient differing pressure needed.

For the simulations it showed to be difficult to get a reliably model in the defined time frame for the project. The principally reason for this is that its been a "trail and error" way of modeling this in ANSYS Workbench 12.1. To gradually increase the complexity of the model was very time consuming and a lot of attempts was needed before any solutions were obtained. But the result gives important information in the evaluation of the software, and highlights the problems that need to be overcome in the future for this type of analysis. There are symmetry planes in the plate pattern that can be exploited to get a time efficient simulation model. But to be able to rely on the information, and have the ability to scale up the result to a full-sized plate, one must overcome the problem with introducing periodic symmetry conditions. These conditions have proved to be needed to provide a reality-based model.

Our simulation do also show that the easiest way to introduce residual stress and plastic strain is by facilitating a multi-step analysis, rather than a script based version with mapped stress and strain. A model with correct symmetry conditions opens up to new analysis where a simulation with and without plastic strain could be compared. Even if the 2D flank simulation shows that the influence of these residuals are small in the region of interrest, it is still a to simple model to give rise to reliable conclusions. The contact point do not reflect the reality and the influence of the inclination angle is not considered.

7.4 Further work

If one wants to perform these tests again it is suggested that they are compressed with respect to the nominal size for that particular nominal assembly length according to the thickness and number of plates. Then one receive the correct load level according to the corresponding assembly length.

The use of multistage analysis is sensitive to if the geometry is changed. Setting up a model for a general plate in this way can be difficult. For example, one parameter like attenuation will change with respect to geometry and may therefore contribute numerical convergence problems caused by contact switches. The preferred way to solve this is with the help of the INISTATE command.

The simulation results and particularly the rhomb model that is modeled on a very small plate area and has a great influence from the restrictive boundary are in need of periodic symmetry conditions. Instead of using a rhomb one could use a rectangular that has the advantage of having orthogonal boundary surfaces.

Bibliography

[1] Gertjan Kloosterman. *Contact methods in finite element simulations.* PhD thesis, Graduate School Engineering Mechanics, Enschede, December 2002.

[2] H. Martin. A theoretical approach to predict the performance of chevron-type plate heat exchangers. *Chemical engineering and processing*, 35(4):301–310, 1996.

[3] N.S. Ottosen and H. Petersson. *Introduction to the finite element method.* Prentice-Hall,, 1992.

[4] N.S. Ottosen and M. Ristinmaa. *The mechanics of constitutive modeling.* Elsevier Science Ltd, 2005.

[5] Arne Persson and Lars-Christer Böiers. *Analys i en variabel.* Studentlitteratur, Lund, 2. uppl. edition, 2001.

[6] RK Shah and WW Focke. Plate heat exchangers and their design theory. *Heat Transfer Equipment Design*, pages 913–932, 1988.

[7] L. Wang, B. Sundén, and RM Manglik. *Plate heat exchangers: design, applications and performance.* Wit Pr/Computational Mechanics, 2007.

Appendix A

ANSYS

A.1 SOLID186

14.186. SOLID186 - 3-D 20-Node Non-Layered/Layered Structural Solid

SOLID186 is available in two forms:

- Standard (nonlayered) structural solid (KEYOPT(3) = 0, the default) - see *Section 14.186.1: SOLID186 - 3-D 20-Node Non-layered Structural Solid*.
- Layered structural solid (KEYOPT(3) = 1) - see *Section 14.186.2: SOLID186 - 3-D 20-Node Layered Structural Solid*.

14.186.1. SOLID186 - 3-D 20-Node Non-layered Structural Solid

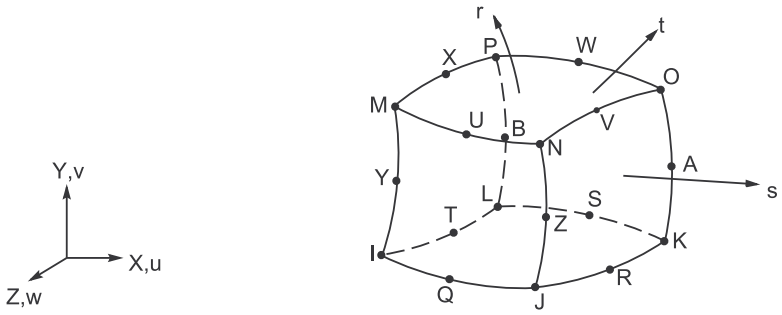

Matrix or Vector	Geometry	Shape Functions	Integration Points
Stiffness and Stress Stiffness Matrices; and Thermal Load Vector	Brick	*Equation 12–209*, *Equation 12–210*, and *Equation 12–211*	14 if KEYOPT(2) = 1 2 x 2 x 2 if KEYOPT(2) = 0
	Wedge	*Equation 12–186*, *Equation 12–187*, and *Equation 12–188*	3 x 3
	Pyramid	*Equation 12–171*, *Equation 12–172*, and *Equation 12–173*	2 x 2 x 2
	Tet	*Equation 12–164*, *Equation 12–165*, and *Equation 12–166*	4
Mass Matrix	Same as stiffness matrix.		3 x 3 x 3 if brick. If other shapes, same as stiffness matrix
Pressure Load Vector	Quad	*Equation 12–69* and *Equation 12–70*	3 x 3
	Triangle	*Equation 12–46* and *Equation 12–47*	6

Load Type	Distribution
Element Temperature	Same as shape functions thru element
Nodal Temperature	Same as shape functions thru element
Pressure	Bilinear across each face

14.186.2. SOLID186 - 3-D 20-Node Layered Structural Solid

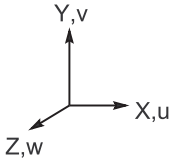

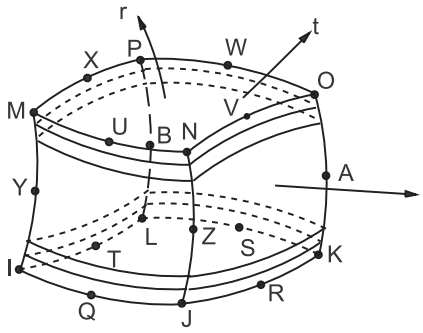

Matrix or Vector	Geometry	Shape Functions	Integration Points
Stiffness and Stress Stiffness Matrices; and Thermal Load Vector	Brick	*Equation 12–209*, *Equation 12–210*, and *Equation 12–211*	In-plane: 2 x 2 Thru-the-thickness: 2 if no shell section defined. 1, 3, 5, 7, or 9 per layer if a shell section is defined
	Wedge	*Equation 12–186*, *Equation 12–187*, and *Equation 12–188*	In-plane: 3 Thru-the-thickness: 2 if no shell section defined. 1, 3, 5, 7, or 9 per layer if a shell section is defined
Mass Matrix	Same as stiffness matrix.		In-plane: 3 x 3 if brick 3 if wedge Thru-the-thickness: Same as stiffness matrix
Pressure Load Vector	Quad	*Equation 12–69* and *Equation 12–70*	3 x 3
	Triangle	*Equation 12–46* and *Equation 12–47*	6

Load Type	Distribution
Element Temperature	Bilinear in plane of element, linear thru each layer
Nodal Temperature	Same as shape functions thru element
Pressure	Bilinear across each face

A.2 SOLID187

14.187. SOLID187 - 3-D 10-Node Tetrahedral Structural Solid

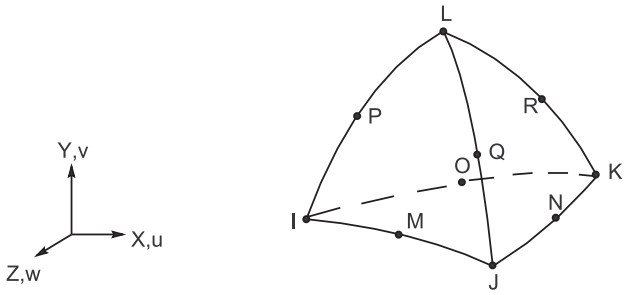

Matrix or Vector	Shape Functions	Integration Points
Stiffness, Mass, and Stress Stiffness Matrices; and Thermal Load Vector	*Equation 12–164*, *Equation 12–165*, and *Equation 12–166*	4
Pressure Load Vector	*Equation 12–164*, *Equation 12–165*, and *Equation 12–166* specialized to the face	6

Load Type	Distribution
Element Temperature	Same as shape functions
Nodal Temperature	Same as shape functions
Pressure	Linear over each face

Reference: Zienkiewicz(*39*)

14.187.1. Other Applicable Sections

Chapter 2: Structures describes the derivation of structural element matrices and load vectors as well as stress evaluations. *Section 3.6: General Element Formulations* gives the general element formulations used by this element.

Appendix B

Blueprints

B.1 Tool design

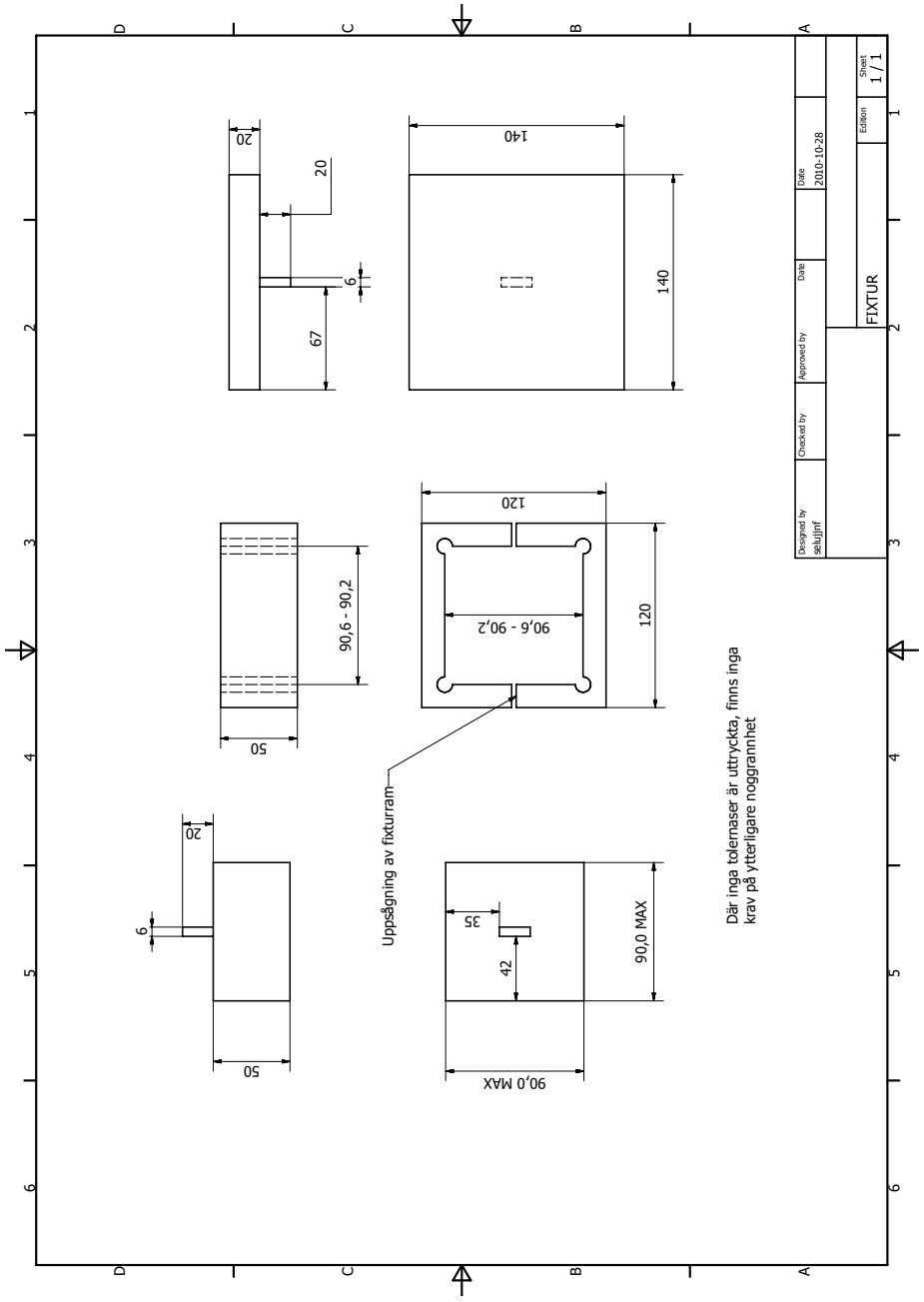

B.2 Water jet plate preperation blueprint

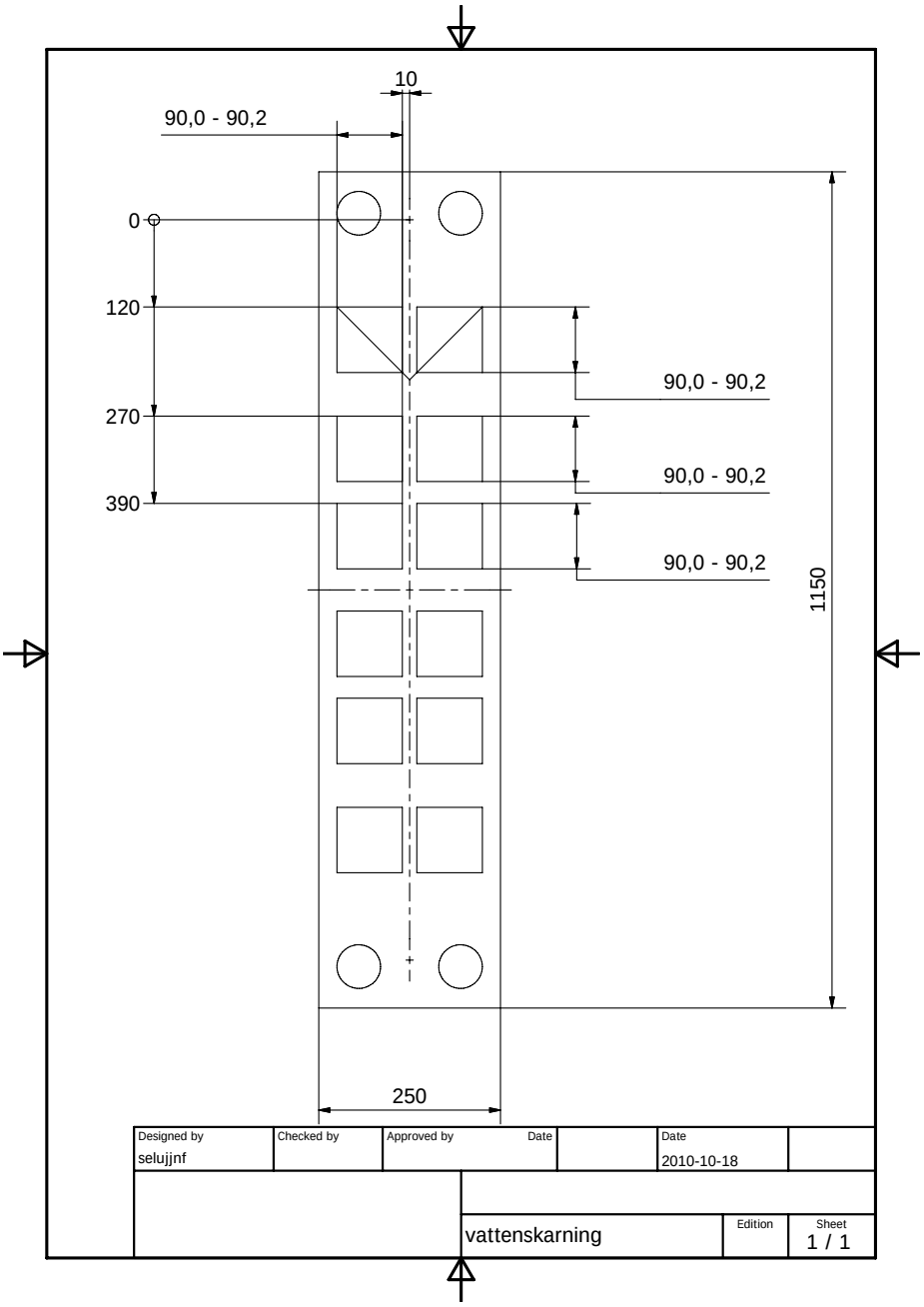

Appendix C

Test

C.1 Test Specification

Test specification

Compression test of GPHE plates

Joel Johansson Henrik Forsbäck

11/30/2010

Contents

Test equipment
All tests are performed in a tensile testing machine, where the machine measures the applied force. The corresponding displacement is manually measured with a dial indicator with its measuring tip set on top of the pressing tool. This due to that the internal position measuring device includes the machine's own internal displacement in the measurement.

Testing procedure
First an initial force of *100 N* is applied to get the dies in contact with the specimen. The tensile test machine is then displacement controlled with a rate of *0.5 mm/min*. One have to notice that this displacement rate is including the internal displacements described prior. The actual displacement rate of the pressing tool is much slower.

Maximum available force from the machine is *35kN*. The range for the tests will thereby be *100-35000 N*.

The dial indicator will be reset after the initial force is applied and then measured every ten second. The actual displacement is then noticed in a test protocol. The calibration protocol, built before the test is attached to this specification as attachments.

In order to be able to test two different procedures a testing tool is produced. This contains of a pressing tool, a reaction support and a detachable boundary box. The first procedure is with the boundary box, the specimens are then limited to expand by the boundary box and shims are installed to have complete contact against the plates. The second procedure is when not using the boundary box allowing the plates to expand.

Test plates
The test plate geometry includes water jet cut specimens from a GPHE plate according to:

Nominal plate thickness	High-theta / Low-theta	Number of specimens
0,4 mm	H	60
0,5 mm	H	60
0,6 mm	H	60
0,4 mm	L	60
0,5 mm	L	60
0,6 mm	L	60

The specimens are distributed as 12 pcs per plate. Each position from where the cut outs are made on the plate is identifiable with the help of a letter and number. Every specimen got an identification number (1-360) that is connected to a *data table* with the measured thickness, the measured pressure depth, position and charge number.

Following notation for the tests is made to know what specimens that are going to be in each test. Example, 0.4HB2. Where

0.4	The thickness is 0,4 mm
H	It is a high-theta plate
B2	The position of the specimen is B2.

Requirements

• Each test is repeated three times to ensure that the result can be repeated.

• Since the pressing tool has an own weight it has to be secured that the measured force is the correct applied force to the plates. Measured force by initial contact to the plate should be zero to fulfill this.

• The charge number for the each plate should be noted so that the material data can be accessed when needed.

Plate measuring

- For each specimen the pressing depth and thickness of the plate will be measured.
- The pressing depth will be an average value from four measuring points presented in figure 1. To avoid errors this measuring is made twice. The average value is added to the data table.
- The thickness is measured on an undeformed area at the original plate. This measured value will then be added to all the specimens on that plate.

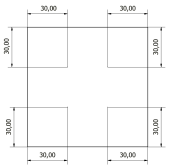

Figure 1 Measuring pressing depth

Test 1: Single plate tests
The test objective is to show how a plate behaves during loading and to illustrate the relationship between applied load and compression of the plate.

This test is performed both with and without boundary box.

The applied force is plotted against the corresponding displacement.
Primary displacement field is *0-0.1mm*.
The testing procedure is followed.

Specimen	**No of tests**	**Boundary box** Y/N
0.4HA1	3	Y
0.4LA1*	3	Y
0.5HA1	3	Y
0.6HA1	3	Y
0.6HA2	3	N

* The low-theta plate test can be excluded. This is performed to display the differences according to different inclination angle.

Test 2: 2 plate tests
The test objective is to relate the different specimens to each other and find out which combination of plates that is the stiffest.

The applied force is plotted against the corresponding displacement.
Primary displacement field is *0-0.1mm* per plate.
The testing procedure is followed.

Plate combination	First plate	No of tests	Second plate	No of tests
High-High theta	0.4HB1	3	0.4HB2	3
Low-Low theta	0.4LB1	3	0.4LB2	3
High-Low theta	0.4HC1	3	0.4LC2	3

Test 3: Multiple plate tests
The test objective with the multiple plate tests is to imitate the assembling of a plate heat exchanger. The plates for these tests are stacked according to the stiffest combination found in test 2. If test 2 not delivers any clear results the multiple plate tests are performed according to the theoretically stiffest combination that should be High/Low-theta.

The applied force is plotted against the corresponding displacement.
Primary displacement field is *0-0.1mm* per plate.
The testing procedure is followed.

Test example

Test	Specimen	No of specimens	Specimen	No of specimens
1	0.5HB2	4	0.5LB1	4
2	0.5HD2	4	0.5LD1	4
3	0.5HF2	4	0.5LF1	4

Test example of three tests made with the number of 8 plates with the thickness of 0.5 mm. The eight plates include four High-theta and four low-theta plates. Stacked High-Low-High-Low and so on.

Test 4: Test material properties
To secure the testing equipment tensile test of raw-material plates were performed. The tensile test machine extrudes the sheet to its maximum load or until the sheet breaks to obtain the most extensive tensile test curve. To verify the result this is repeated three times.

It is important that the sheet material is placed in the machine in a proper direction to just obtain normal tension and no shearing.

Appendix D

Calibration records

D.1 Schenk RM - 100

Duro - Tensile service ab

SWEDAC ACKREDITERING 1723 ISO/IEC 17025

KALIBRERINGSBEVIS
utfärdat av ackrediterat laboratorium
CALIBRATION CERTIFIKATE issued by an Accredited Laboratory

Bevisnr. 006859 Sida.1(1)
Utfärdat av Vendel Kisch
Resultaten avser endast de föremål som är specificerade i detta dokument
Uppdragsgivare. Materials & Chemistry Centre MACC 221 00 Lund
Er referens Martin Johansson

Kontrollobjekt :

Fabrikat, typ, tillv.nr.	Schenk RM – 100	A.nr. 41.273
Uppställningsplats.	Materiallabb	
Mätdon nr.	-	
Kraftalstring.	Mekaniskt	
Kraftmätning.	Pc	Styrsystem TRM-100
Kontrollerade mätområden.	100, 40 och 200 ton	Drag
Kalibreringsprincip.	Jämförelsemätning mot kalibrerad normal(er)	

Uppdrag den 13 maj 2009 utfördes kontroll av kraftmätningssystem på ovannämnda föremål enligt SS-EN ISO 7500-1 : 2004

Temperatur vid kontrollen 22,8 °C

Använda kontrollutrustning

	Typ	Tillv.nr.	Kal.bevis	Kal.datum.	Klass
Digital lastindikator	PM-G4	06-1046	-	-	-
Lastcell 100 kN	KSG-3	99100	1156-09010	2009-02-10	1
Lastcell 10 kN	VT-620	50095624	1156-09007	2009-02-08	1
Lastcell 2,5 kN	LC 101-500	169943	1156-09006	2009-01-23	1

Spårbarhet
Kontrollinstrument och lastcell är genom regelbunden kalibrering av Vishay Nobel med spårbarhet till RMP01 kraftnormal via Nobel 1156.

Resultat
Erhållna resultat från kontrollen redovisas i bilaga.

Mätosäkerhet vid kalibreringen
Den angivna utvidgade mätosäkerheten är produkten av standardmätosäkerheten och täckningsfaktorn k=2 vilket för en normalfördelning svarar mot en täckningssannolikhet av ungefär 95%. Standardmätosäkerheten har bestämts

i enlighet med EAs publikation EA-4/02 Begränsningar av standard: ingen
Datorberäkningar enl Excel version 9.0.2812 (dok 5.10.8-Dpr. utg.1.)

Provningsmaskinens klass
Maskinen uppfyller kraven enligt ISO 7500-1 för nedan specificerade provkrafter och för nedan angiven maskinklas.

Typ	Mätområde	Klassintervall	Klass
Drag	0 - 50000 N	5000 - 50000 N	1
Drag	0 - 50000 N	500 - 1500 N	2
Drag	0 - 50000 N	1500 - 5000 N	1

Ansvarig för mätningen
Vendel Kisch

Bilaga Kontrollresultat (1 sida/or)

Ackrediterat laboratorium utses av Styrelsen för teknisk ackreditering (SWEDAC) enligt lag. Verksamheten vid de svenska ackrediterade laboratorierna uppfyller kraven i SS-EN ISO/IEC 17025.

Duro - Tensile
service ab

SWEDAC ACKREDITERING 1722 ISO/IEC 17025

Bilaga till kalibreringsbevis nr. 006859 **Sidan 1(1)**

RESULTAT AV KONTROLLEN

ISO 7500-1avsnitt 9 anger att intervallen mellan två kontrolltillfällerna bör ej överskrida 12 månader.
Om maskinen flyttas, repareras eller justeras måste den kontroleras på nytt.

Allmän granskning av provningsmaskinens tillstånd

1.1 Syning

Inga anmärkningar.

1.2 Granskning av maskinens konstruktion.

Inga anmärkningar.

1.3 Granskning av kraftpåförande styrsystem.

Inga anmärkningar.

Mätområde för max kraft **50000 N-Drag**

Maskinen visar (Fi)N	Verklig kraft (F)N	Relativ onoggrannhet (q) %	Relativ repeterbarhet (b) %	Relativ upplösning (a) %	Mätosäkerhet	
					Relativ (U)%	Absolut (U)N
5000,0	5015,3	-0,31	0,18	0,00	0,33	16,5
10000,0	9990,3	0,10	0,31	0,00	0,38	38,0
15000,0	14984,0	0,11	0,35	0,00	0,43	64,5
20000,0	19991,7	0,04	0,36	0,00	0,45	90,0
25000,0	24984,3	0,06	0,34	0,00	0,44	110,0
30000,0	29993,0	0,02	0,28	0,00	0,39	117,0
35000,0	34997,7	0,01	0,26	0,00	0,39	136,5
40000,0	40000,7	0,00	0,26	0,00	0,39	156,0
45000,0	45004,7	-0,01	0,22	0,00	0,38	171,0
50000,0	50017,0	-0,03	0,22	0,00	0,39	195,0
0,0	0,0	1)				

1) Relativt nollpunktsfel, f_0 = 0,1% av maximala provkraft

Mätområde för max kraft **5000 N-Drag**

Maskinen visar (Fi)N	Verklig kraft (F)N	Relativ onoggrannhet (q) %	Relativ repeterbarhet (b) %	Relativ upplösning (a) %	Mätosäkerhet	
					Relativ (U)%	Absolut (U)N
500,0	505,3	-1,06	1,19	0,02	1,38	6,9
1000,0	1010,0	-0,99	1,98	0,01	2,29	22,9
1500,0	1512,7	-0,84	0,99	0,01	1,16	17,4
2000,0	2006,0	-0,30	0,30	0,00	0,37	7,4
2500,0	2514,7	-0,58	0,48	0,00	0,57	14,3
3000,0	3016,0	-0,53	0,40	0,00	0,49	14,7
3500,0	3511,0	-0,31	0,09	0,00	0,34	11,9
4000,0	4015,3	-0,38	0,45	0,00	0,55	22,0
4500,0	4514,3	-0,32	0,35	0,00	0,44	19,8
5000,0	5015,7	-0,31	0,12	0,00	0,32	16,0
0,0	0,0	1)				

1) Relativt nollpunktsfel, f_0 = 0,1% av maximala provkraft